Supplementary Information for

Liquid Coordination Polymers with Anhydrous Proton Conductivity

Nattapol Ma,* Soracha Kosasang, Satoshi Horike, and Hiroki Yamada

Correspondence to: ma.nattapol@nims.go.jp

Methods

Synthesis of dehydrated $Zn_3(H_2PO_4)_6(H_2O)_3$](1,2,3-benzotriazole) (ZnPBTA)

ZnO (99.99% trace metals basis), phosphoric acid (85% in H_2O), and 1,2,3-benzotriazole (>98.0%, HPLC) were purchased from Sigma Aldrich, FUJIFILM Wako Pure Chemical, and Tokyo Chemical Industry, respectively. All chemicals were used without further purification. Zinc oxide (1281.7 mg, 15.75 mmol), 1,2,3-benzotriazole (625.4 mg, 5.25 mmol), and phosphoric acid (31.5 mmol, 2163 µL) were added to a 25 mL Teflon jar with two steel-cored 10 mm Teflon balls. The mixer was milled for 60 min at 25 Hz using a Retsch MM 400 mixer mill. The dehydrated sample was obtained after drying at 70 °C for 12 h under vacuum (labeled as ZnPBTA) and kept in an Ar-filled glovebox to prevent adsorption of moisture. The vacuum pump used for dehydration process is TSW-150, SATO VAC INC.

Synthesis of ZnPBTA-m1

ZnO (99.99% trace metals basis), phosphoric acid (85% in H_2O), and 1,2,3-benzotriazole (>98.0%, HPLC) were purchased from Sigma Aldrich, FUJIFILM Wako Pure Chemical, and Tokyo Chemical Industry, respectively. All chemicals were used without further purification. Zinc oxide (1281.7 mg, 15.75 mmol), 1,2,3-benzotriazole (625.4 mg, 5.25 mmol), and phosphoric acid (40.7 mmol, 2794 µL) were added to a 25 mL Teflon jar with two steel-cored 10 mm Teflon balls. The mixer was milled for 60 min at 25 Hz using a Retsch MM 400 mixer mill. The dehydrated sample was obtained after drying at 70 °C for 12 h under vacuum (labeled as ZnPBTA-m1) and kept in an Ar-filled glovebox to prevent adsorption of moisture.

Synthesis of ZnPBTA-m2

ZnO (99.99% trace metals basis), phosphoric acid (85% in H_2O), and 1,2,3-benzotriazole (>98.0%, HPLC) were purchased from Sigma Aldrich, FUJIFILM Wako Pure Chemical, and Tokyo Chemical Industry, respectively. All chemicals were used without further purification. Zinc oxide (1281.7 mg, 15.75 mmol), 1,2,3-benzotriazole (625.4 mg, 5.25 mmol), and phosphoric acid (49.9 mmol, 3425 µL) were added to a 25 mL Teflon jar with two steel-cored 10 mm Teflon balls. The mixer was milled for 60 min at 25 Hz using a Retsch MM 400 mixer mill. The dehydrated sample was obtained after drying at 70 °C for 12 h under vacuum (labeled as ZnPBTA-m2) and kept in an Ar-filled glovebox to prevent adsorption of moisture.

Synthesis of ZnPBTA-m3

ZnO (99.99% trace metals basis), phosphoric acid (85% in H_2O), and 1,2,3-benzotriazole (>98.0%, HPLC) were purchased from Sigma Aldrich, FUJIFILM Wako Pure Chemical, and Tokyo Chemical Industry, respectively. All chemicals were used without further purification. Zinc oxide (1281.7 mg, 15.75 mmol), 1,2,3-benzotriazole (625.4 mg, 5.25 mmol), and phosphoric acid (59.1 mmol, 4056 µL) were added to a 25 mL Teflon jar with two steel-cored 10 mm Teflon balls. The mixer was milled for 60 min at 25 Hz using a Retsch MM 400 mixer mill. The dehydrated sample was obtained after drying at 60 °C for 12 h under vacuum (labeled as ZnPBTA-m3) and kept in an Ar-filled glovebox to prevent adsorption of moisture.

Powder X-ray diffraction (PXRD)

Powder X-ray diffraction (PXRD) patterns were collected using a Rigaku MiniFlex with a CuKα anode (45 kV, 50 mA) (λ = 1.5406 Å). Samples were mounted on a low-background silicon sample holder and measured between the 2θ range of 5° to 45° with a step size of 0.02°. Air-sensitive sample holder (Rigaku) was used for the ZnPBTA-g, ZnPBTA-g-m1, ZnPBTA-g-m2, and ZnPBTA-g-m3.

Magic-angle spinning nuclear magnetic resonance (MAS NMR)

^{31}P MAS Solid-state NMR (600 MHz) was performed on a JNM-ECZ600R (JEOL RESONANCE Inc.) solid-state NMR spectrometer at 14.1 T at room temperature at 20 kHz (3.2 mm rotor). All samples were prepared in the Ar-filled glovebox and measured using the single pulse method for 8 scans with a relaxation time of 300 s.

Inductively Coupled Plasma-Optical Emission Spectroscopy (ICP-OES)

ICP-OES measurements were performed using an Agilent 5800 instrument (Agilent Technologies Ltd.). Samples were digested with sulfuric acid and nitric acid and diluted prior to analysis. A Y standard solution was added as an internal standard.

Fourier-transform infrared spectroscopy (FTIR)

IR spectra were collected using Bruker ALPHA Compact FT-IR Spectrometer equipped with Universal ATR accessory. The equipment was installed inside Ar-filled glovebox.

Synchrotron X-ray total scattering

Each sample was filled into a Lindemann glass capillary with an outer diameter of 1.0 mm and sealed using ceramic glues. The synchrotron X-ray total scattering was collected on the BL04B2 beamline at the Super Photon ring-8 GeV (SPring-8, Hyogo, Japan). The energy of the incident beam is 112.9232 keV (λ = 0.109795 Å). The exposure time is 600 s. Scattering data from an empty capillary with an outer diameter of 1.0 mm were used for the background subtraction. Correction for absorption, polarization, background, Compton scattering, and normalization for the Faber−Ziman total structure factor $S(Q)$ were conducted using the BL04B2 analysis program v15 package equipped with SFF_CSF v04.1 software package running on Igor Pro ver9.05. The software is an in-house software developed for the BL04B2 beamline (SPring-8).[1] The pair distribution function (PDF) was calculated by Fourier transforming the normalized $S(Q)$ with a Lorch modification function.[1-3]

Simulated PDF patterns and partial PDFs were calculated using PDFgui software.[4] The model crystal structure of ZnPBTA was taken from ref. [5].

Thermogravimetric and calorimetric analysis

Thermogravimetric analysis (TGA) results were obtained using a Rigaku Thermo plus TG 8121 with a heating rate of 10 °C min^{-1} under flowing Ar (35 mL/min). The measurements were conducted in Al pans from 30 to 500 °C.

Differential Scanning Calorimetry (DSC) was collected using the Hitachi DSC7020 under a flowing N_2 atmosphere with a heating rate of 10 °C min^{-1}. The measurements were conducted using Pt pans. The peak melting temperature ($T_{m,\,peak}$) was assigned at the temperature at the peak of the DSC curve with the endset temperature described in Table S3.

Energy-dispersive spectroscopy (EDS)

Energy-dispersive X-ray spectroscopy (EDS) was performed using a field-emission scanning electron microscope (FE-SEM, SU-8000, Hitachi High-Technologies Corporation) equipped with a Bruker FlatQUAD EDS detector (operated using 12 kV filter). Samples were mounted on the holder using carbon tape (NISSHIN EM Co., Ltd.) and analyzed without metal sputter coating.

Viscosity measurements

Temperature-dependent viscosity results were collected using a rotational parallel-plate rheometer (Discovery Hybrid Rheometer HR20 – TA instruments) under dry N_2 flow, applying an oscillatory strain of 1% at the frequency of 1 Hz. Prior to measurement, the samples were heated to 393 K under dry N_2 and measured without further exposure to ambient air, ensuring minimal contribution from residual water.

Proton conductivity

Conductivity measurements were performed using the electrochemical impedance spectroscopy (EIS) technique. Samples were filled into the conductivity cell with a fixed dimension above their melting temperature (393 K) and quenched to room temperature. The temperature is above the melting temperature of all samples and the boiling point of water, ensuring minimal contribution from residual water. All preparation steps were conducted in an Ar-filled glovebox with a humidity level below 1 ppm. All measurements were performed in a temperature-controlled environment in a closed system filled with dry Ar gas. The measurements were collected using a BioLogic SP-300 potentiostat over a frequency range of 1 MHz to 0.1 Hz with an input voltage amplitude of 100 mV. The collected data were analyzed using EC-Lab software V11.33 via equivalent circuit fitting.

The EIS data for the unmodified ZnPBTA and ZnPBTA-g were analyzed using the $R_1 + R_2Q_1$ equivalent circuit model, where R_1 represents the bulk resistance of the sample, and R_2Q_1 corresponds to the interfacial resistance and constant phase element associated with the electrode–electrolyte interface. For the ZnPBTA-g-m1, ZnPBTA-g-m2, and ZnPBTA-g-m3, the impedance spectra exhibited additional features in the frequency region related to interfacial processes that could not be adequately reproduced using the original $R_1 + (R_2Q_1)$ model. To account for this, an additional interfacial element (R_3Q_2) was introduced, resulting in a better-converged fit. The proton conductivities of the samples were subsequently calculated using the bulk resistance (R_1) obtained from the fitted circuit and calculated using the following equation:

$$\sigma = \frac{L}{(R) \times \pi r^2}$$

L represents the thickness of the pellet, *R* is the resistance, and *r* is the pellet radius.

Density measurement

The density of the melt-quenched samples was measured using the AccuPycII N_2 gas pycnometer at 298 K. To prevent corrosion from the acidic nature of the samples, they were melt-quenched into customized PEEK containers (one-sided open) within an Ar-filled glovebox, avoiding direct contact with the instrument. The volume of the PEEK containers was measured prior to the sample measurements, and the sample volumes were determined by subtracting the container volume from the total measured volume. Each measurement consisted of 10 cycles with an equilibration rate of 0.0345 kPa_g/min.

Supplementary figures

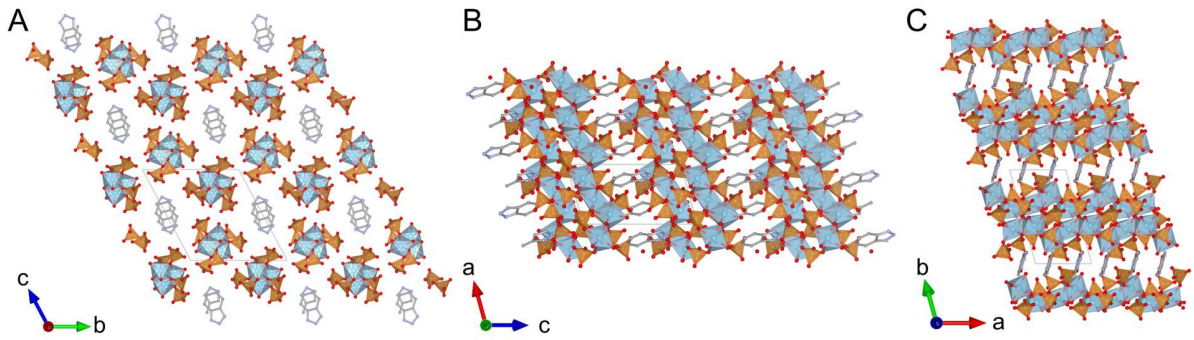

Figure S1. Crystal structure of ZnPBTA.[5] Packing structure on the (A) *bc*-plane, (B) *ac*-plane, and (C) *ab*-plane. Zn, P, O, C, and N atoms are represented by blue (polyhedral), orange (polyhedral), red, grey, and blue spheres, respectively. H atoms are omitted for clarity.

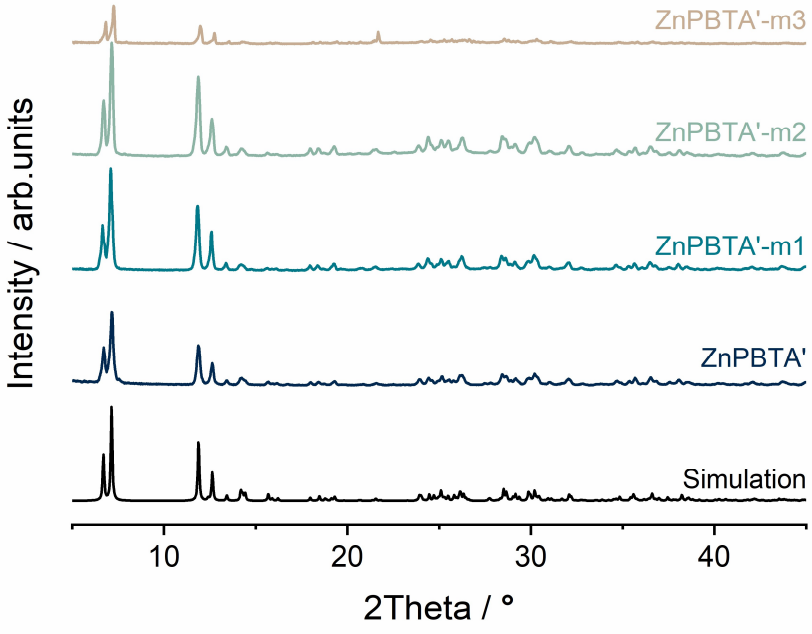

Figure S2. PXRD patterns of ZnPBTA', ZnPBTA'-m1, ZnPBTA'-m2, and ZnPBTA'-m3 before dehydration and the simulated PXRD pattern of ZnPBTA (ref. [5]). λ = 1.5406 Å.

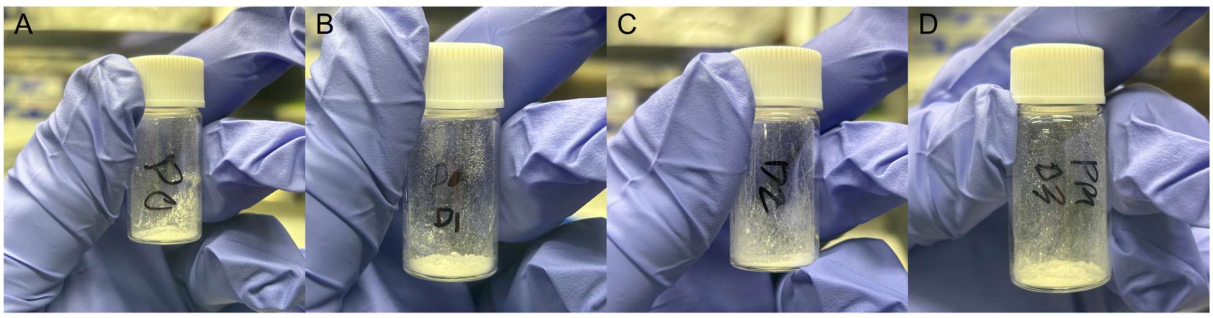

Figure S3. Photographs of the (A) ZnPBTA, (B) ZnPBTA-m1, (C) ZnPBTA-m2, and (D) ZnPBTA-m3.

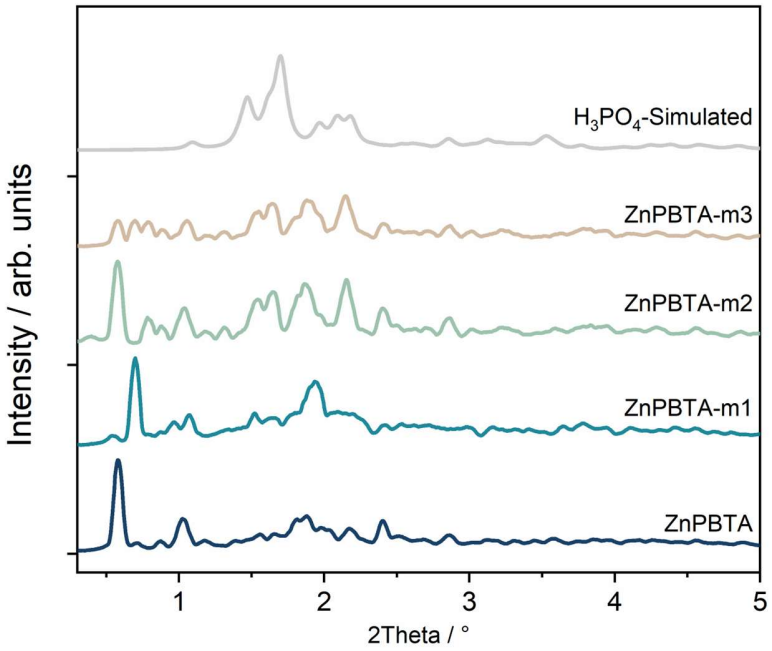

Figure S4. PXRD patterns of ZnPBTA, ZnPBTA-m1, ZnPBTA-m2, and ZnPBTA-m3 after dehydration and the simulated PXRD pattern of H_3PO_4 (ref. [6]). λ = 0.109795 Å. No peaks corresponding to crystalline H_3PO_4 were observed.

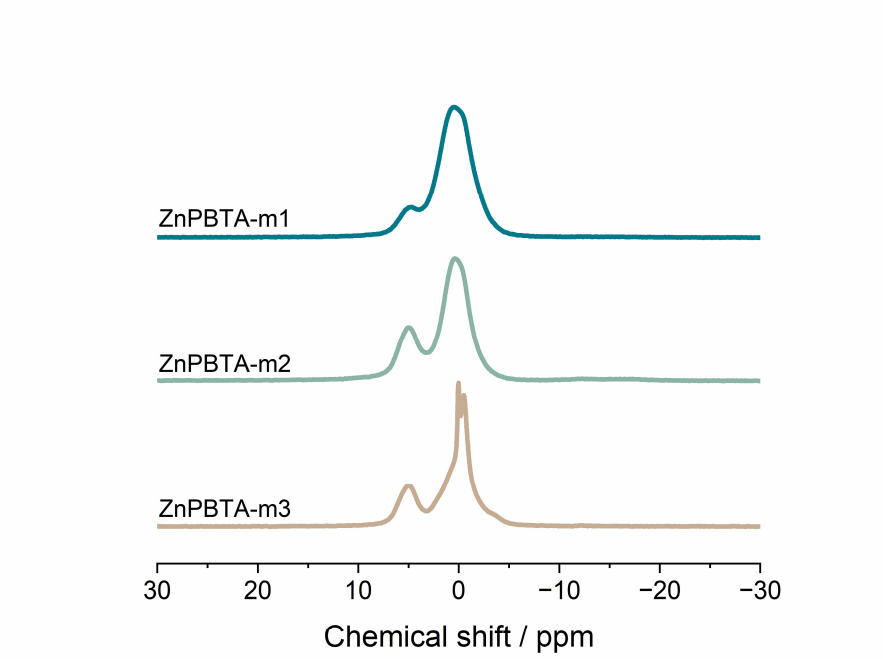

Figure S5. ^{31}P Magic-angle spinning (MAS) NMR spectrum of ZnPBTA-m1, ZnPBTA-m2, and ZnPBTA-m3 at 20 kHz.

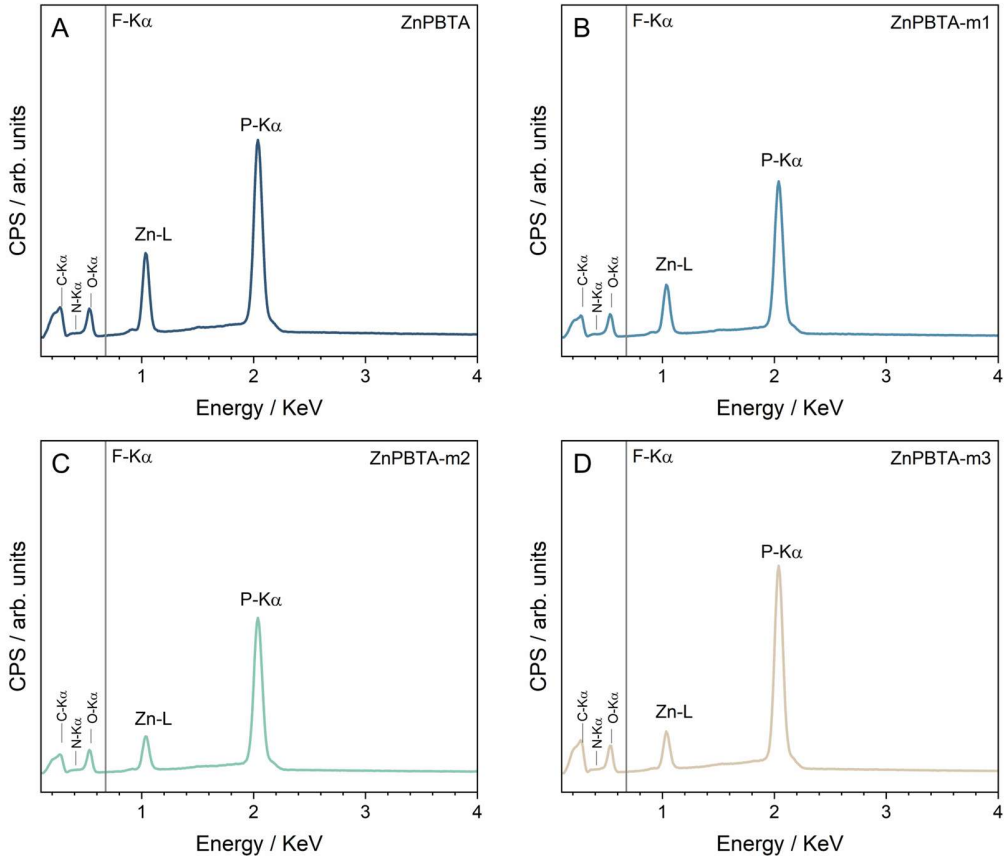

Figure S6. Energy-Dispersive Spectroscopy (EDS) spectra of ZnPBTA, ZnPBTA-m1, ZnPBTA-m2, and ZnPBTA-m3. The absence of a characteristic peak in the F-Kα region confirms that no Teflon abrasion occurred.

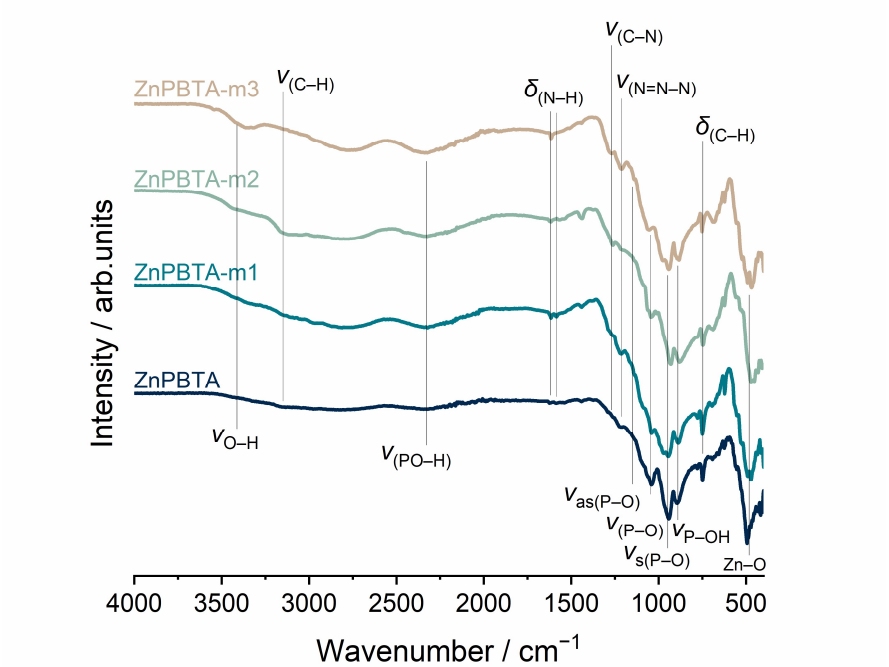

Figure S7. FTIR of ZnPBTA, ZnPBTA-m1, ZnPBTA-m2, and ZnPBTA-m3 under Ar atmosphere. Peak assignments are based on ref. [7-10].

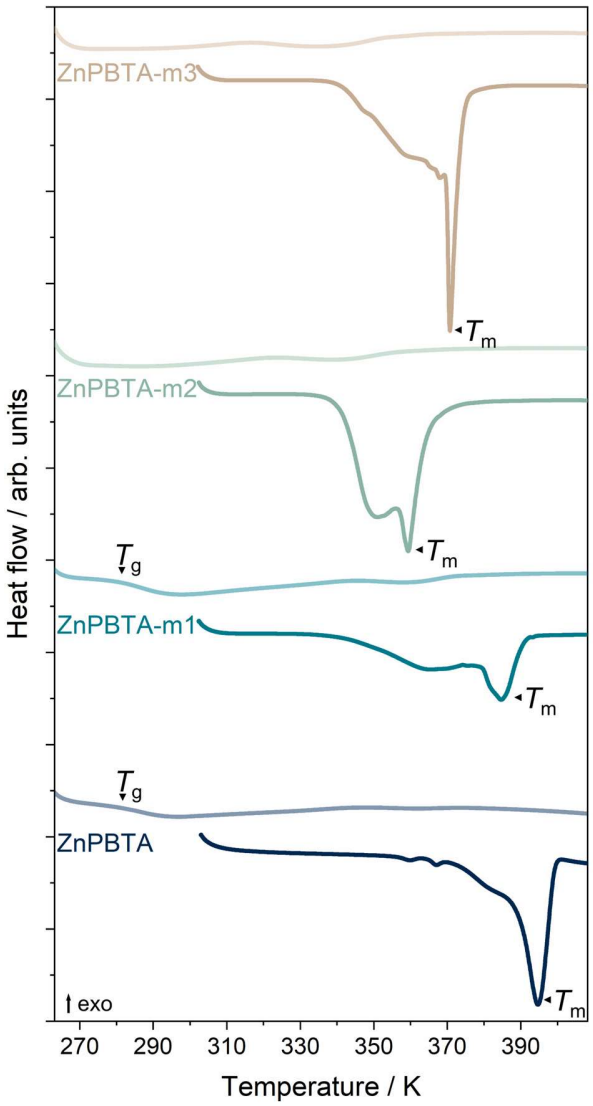

Figure S8. First and second heating DSC profiles of ZnPBTA, ZnPBTA-m1, ZnPBTA-m2, and ZnPBTA-m3 (from bottom to top). The measurements begin with a heating step from 303 K. Detailed information on the melting temperatures and enthalpies associated with the melting peaks is provided in Table S3.

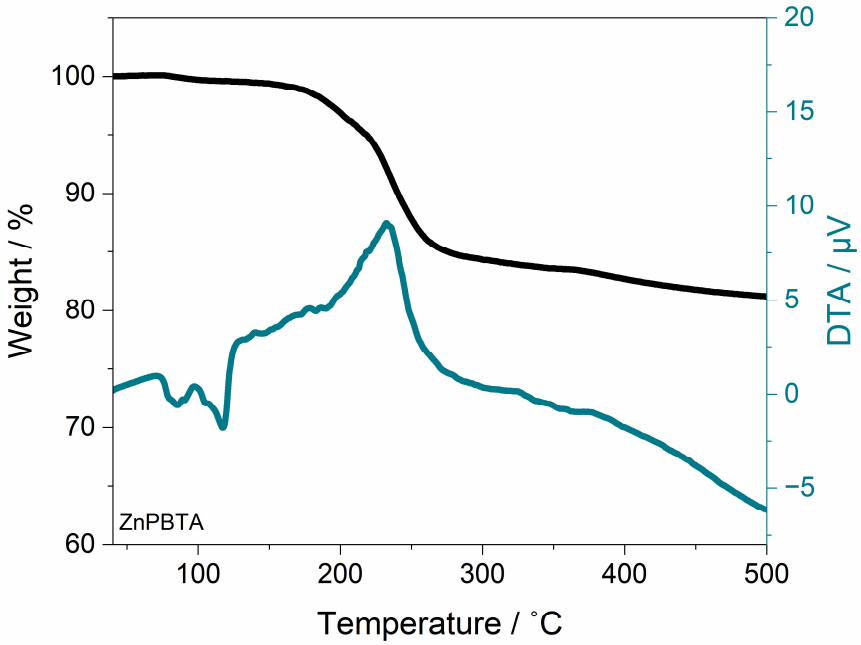

Figure S9. TGA and DTA of ZnPBTA under Ar atmosphere with a heating rate of 10 K min^{-1}.

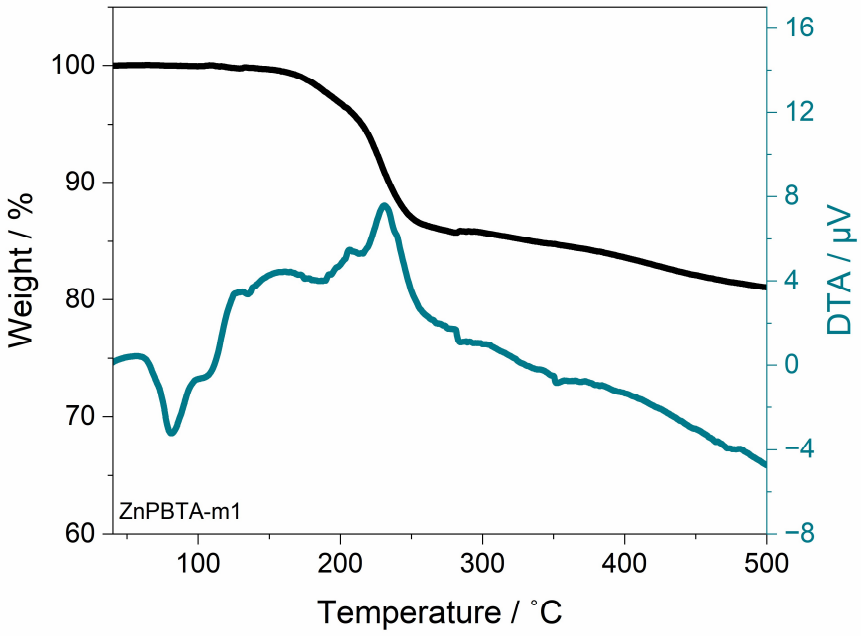

Figure S10. TGA and DTA of ZnPBTA-m1 under Ar atmosphere with a heating rate of 10 K min^{-1}.

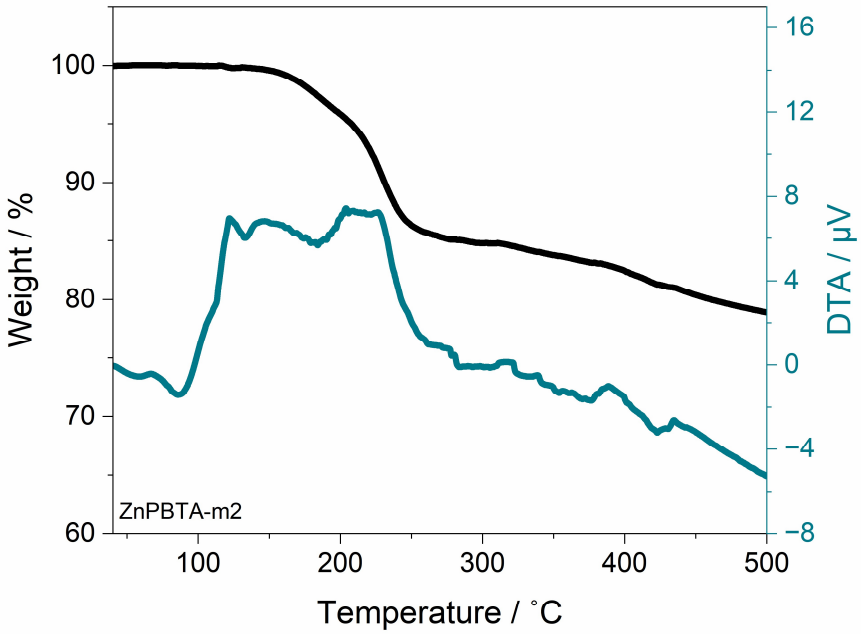

Figure S11. TGA and DTA of ZnPBTA-m2 under Ar atmosphere with a heating rate of 10 K min^{-1}.

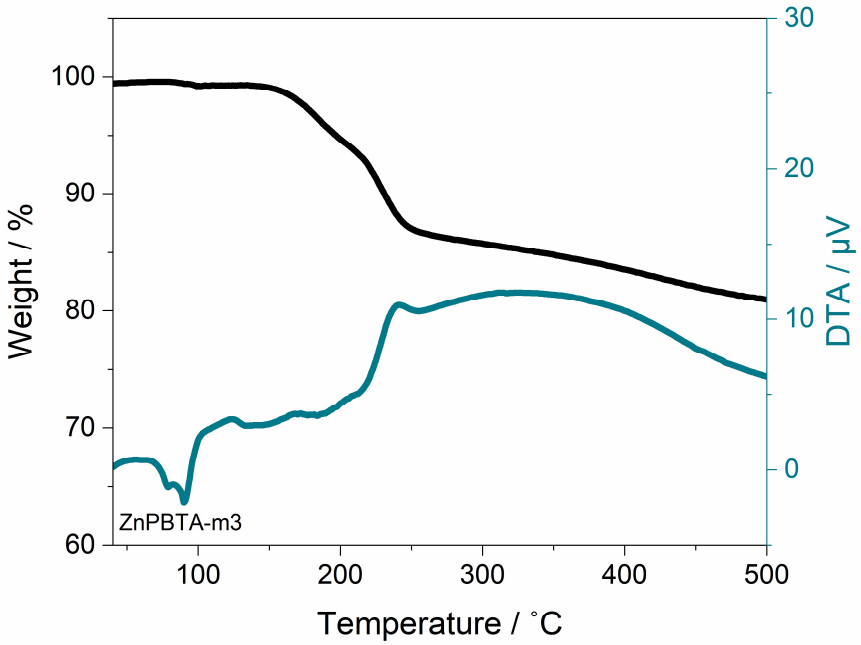

Figure S12. TGA and DTA of ZnPBTA-m3 under Ar atmosphere with a heating rate of 10 K min^{-1}.

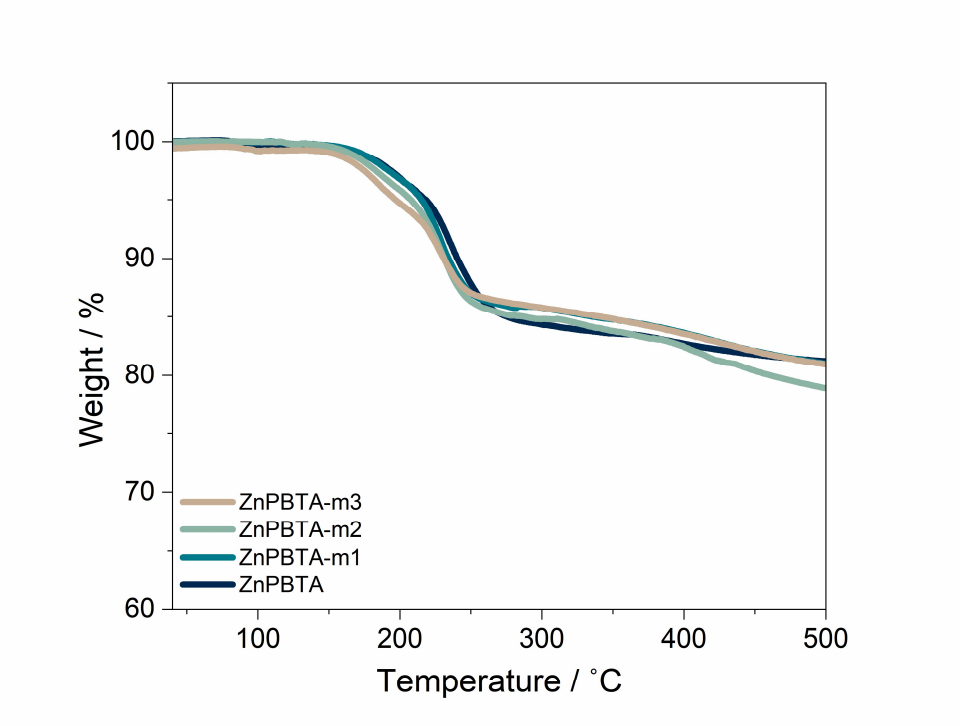

Figure S13 Overlay TGA profiles of ZnPBTA, ZnPBTA-m1, ZnPBTA-m2, and ZnPBTA-m3 under Ar atmosphere with a heating rate of 10 K min^{-1}. Residual coordinated water is expected to be completely released at 120 °C (393 K). Based on this, the estimated water content in ZnPBTA, ZnPBTA-m1, ZnPBTA-m2, and ZnPBTA-m3 is ca. 0.4 wt%, 0.1 wt%, 0.1 wt%, and 0.8 wt%, respectively.

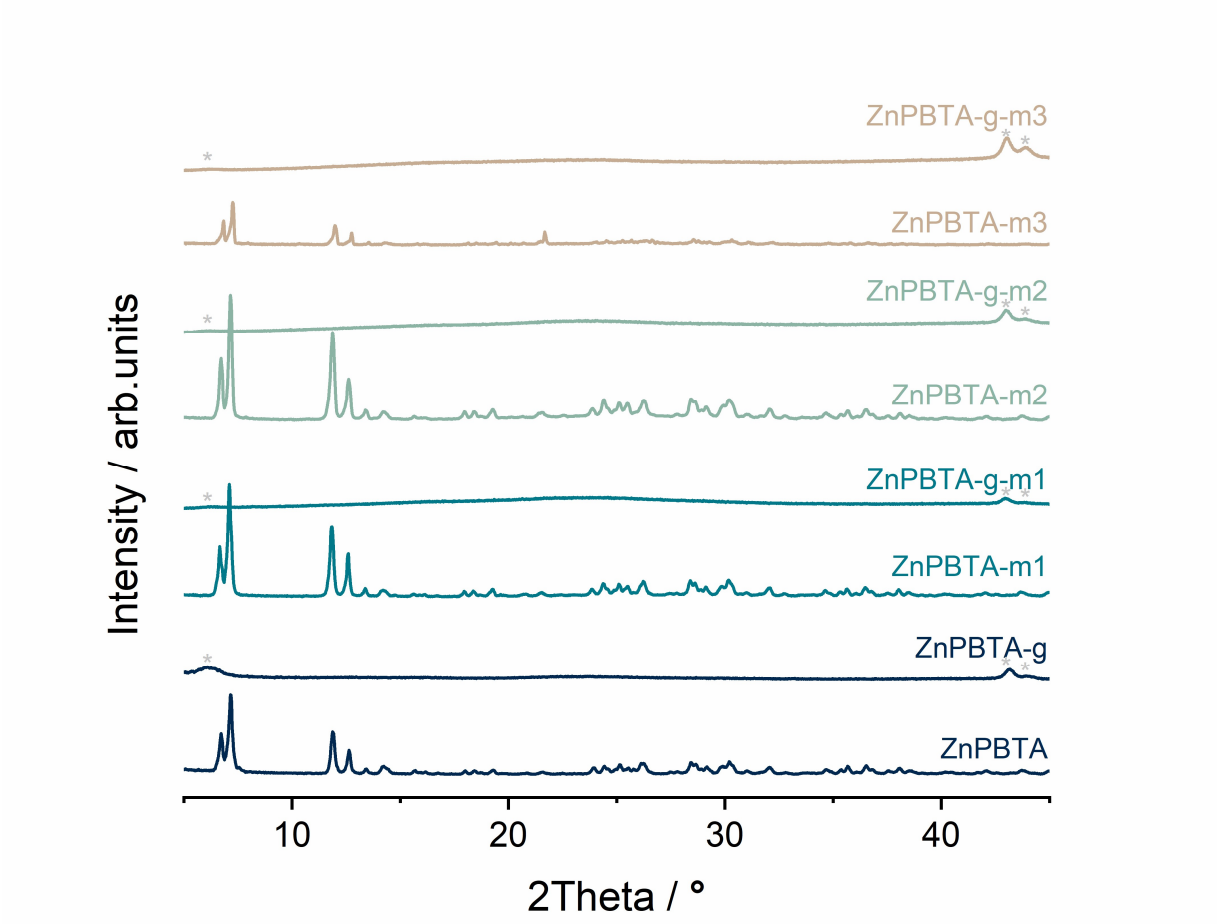

Figure S14. PXRD patterns of melt-quenched ZnPBTA-g, ZnPBTA-g-m1, ZnPBTA-g-m2, and ZnPBTA-g-m3 in comparison with the original samples before dehydration and melt-quenching. Data of ZnPBTA and ZnPBA-g are taken from ref. [5]. Air-sensitive sample holder cell background peaks represented as (*).

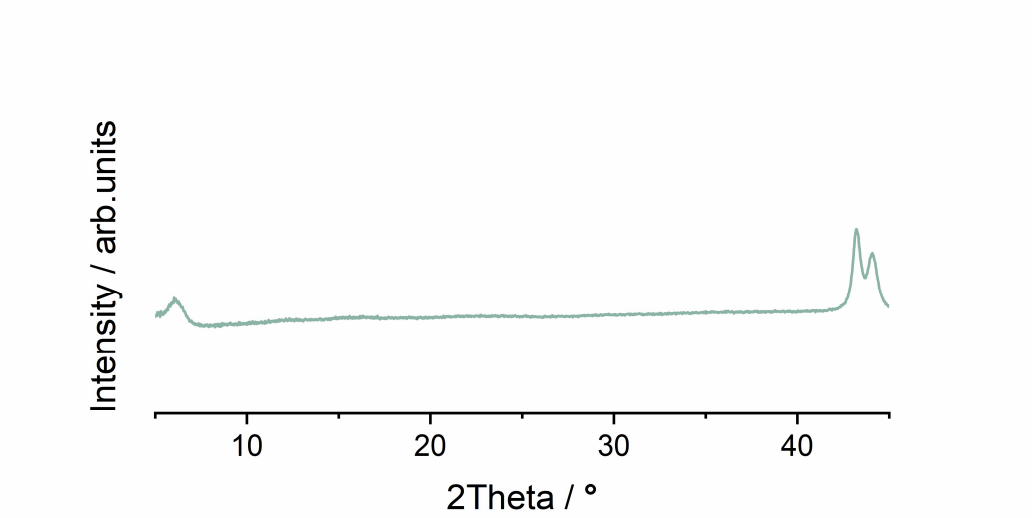

Figure S15. PXRD pattern of the air-sensitive sample holder cell without sample.

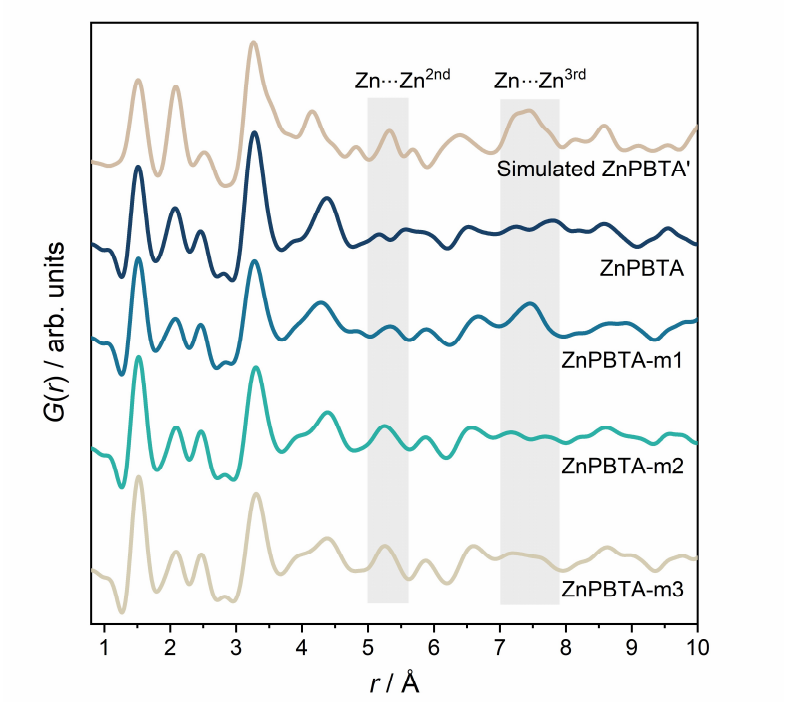

Figure S16. Pair distribution function (PDF) of ZnPBTA, ZnPBTA-m1, ZnPBTA-m2, ZnPBTA-m3, and simulated PDF pattern of ZnPBTA'.

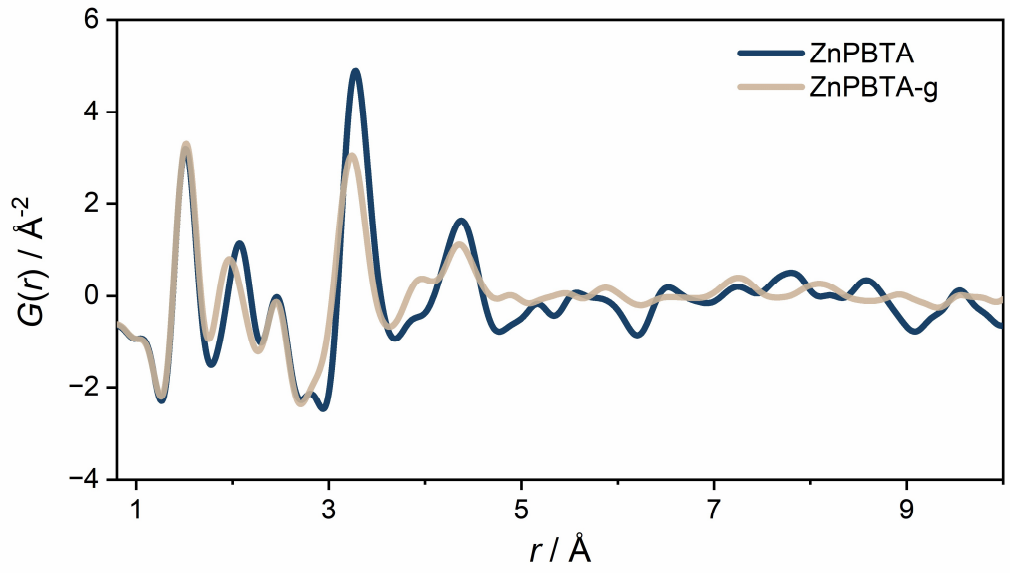

Figure S17. Pair distribution function (PDF) of ZnPBTA and ZnPBTA-g. Note that ZnPBTA-g exhibits a small degree of recrystallization due to its fast crystallization under ambient conditions.[11]

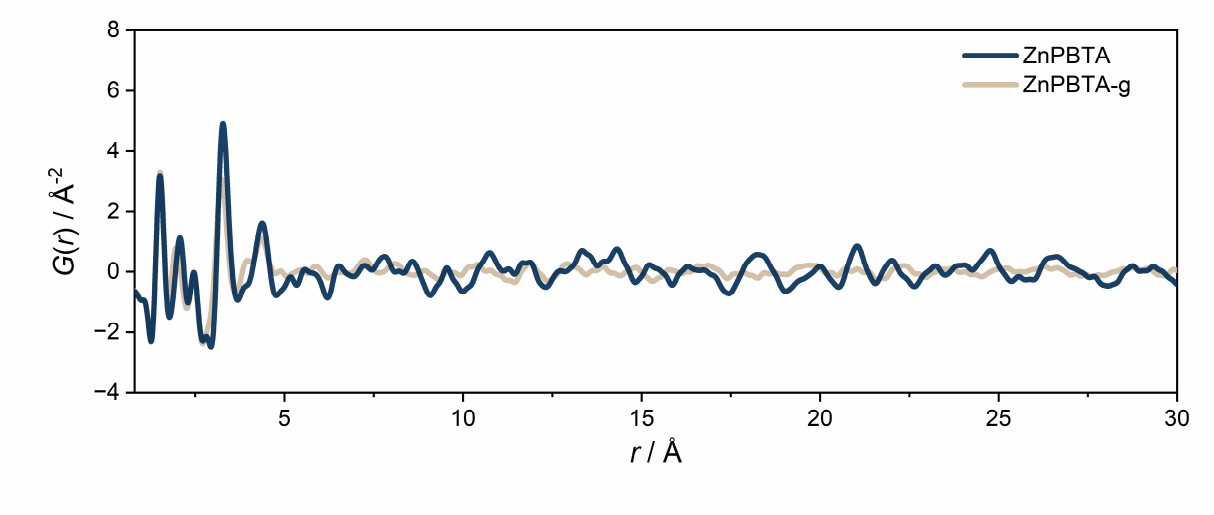

Figure S18. Pair distribution function (PDF) of ZnPBTA and ZnPBTA-g with extended range. Note that ZnPBTA-g exhibits a small degree of recrystallization due to its fast crystallization under ambient conditions.[11]

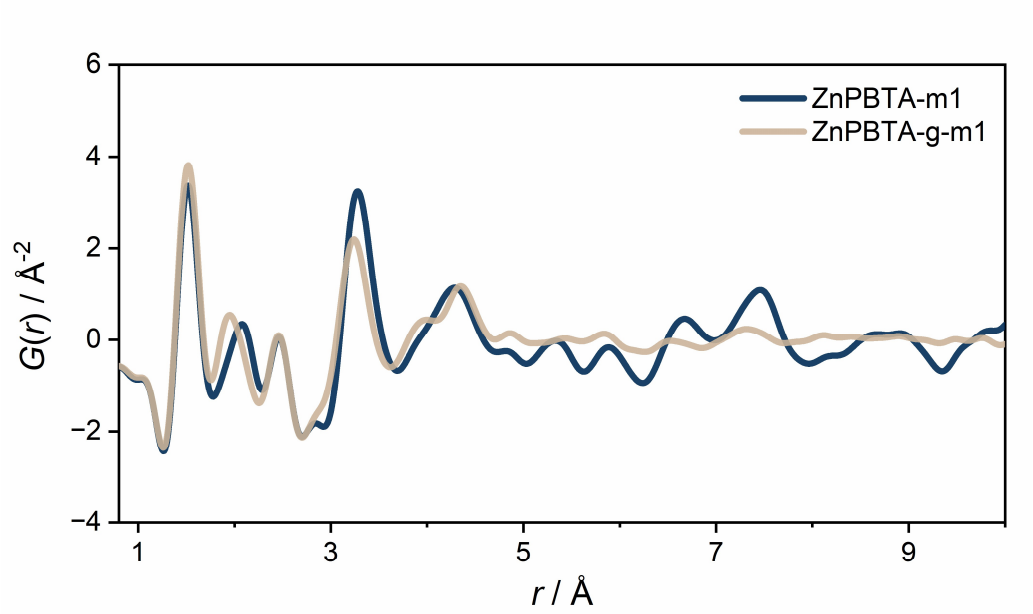

Figure S19. Pair distribution function (PDF) of ZnPBTA-m1 and ZnPBTA-g-m1.

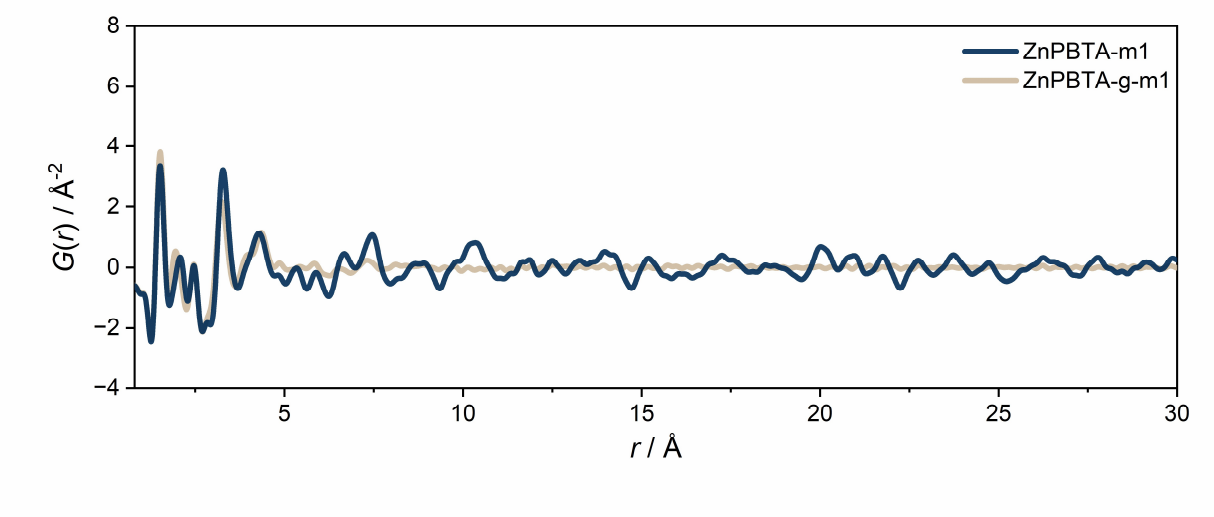

Figure S20. Pair distribution function (PDF) of ZnPBTA-m1 and ZnPBTA-g-m1 with extended range.

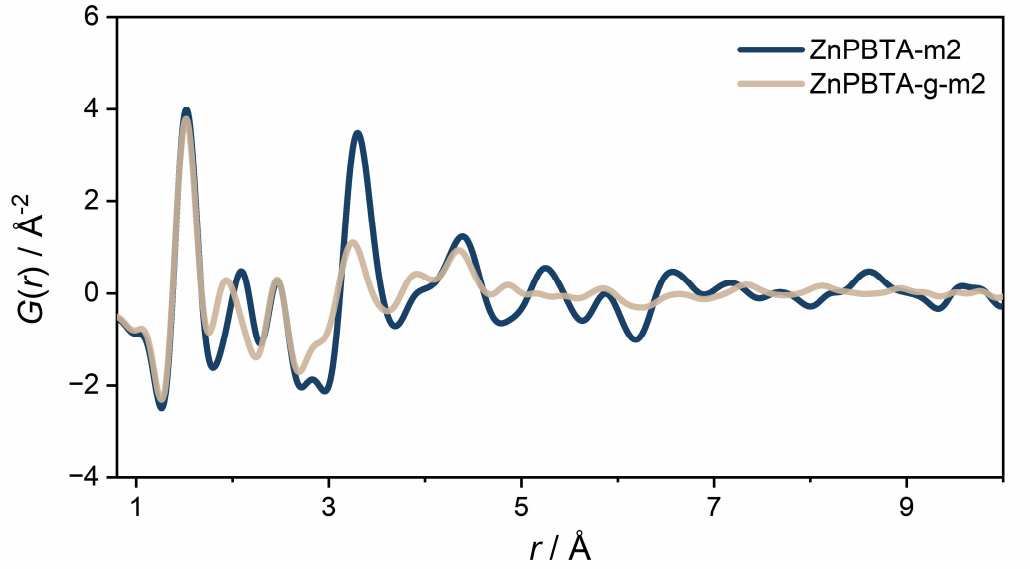

Figure S21. Pair distribution function (PDF) of ZnPBTA-m2 and ZnPBTA-g-m2.

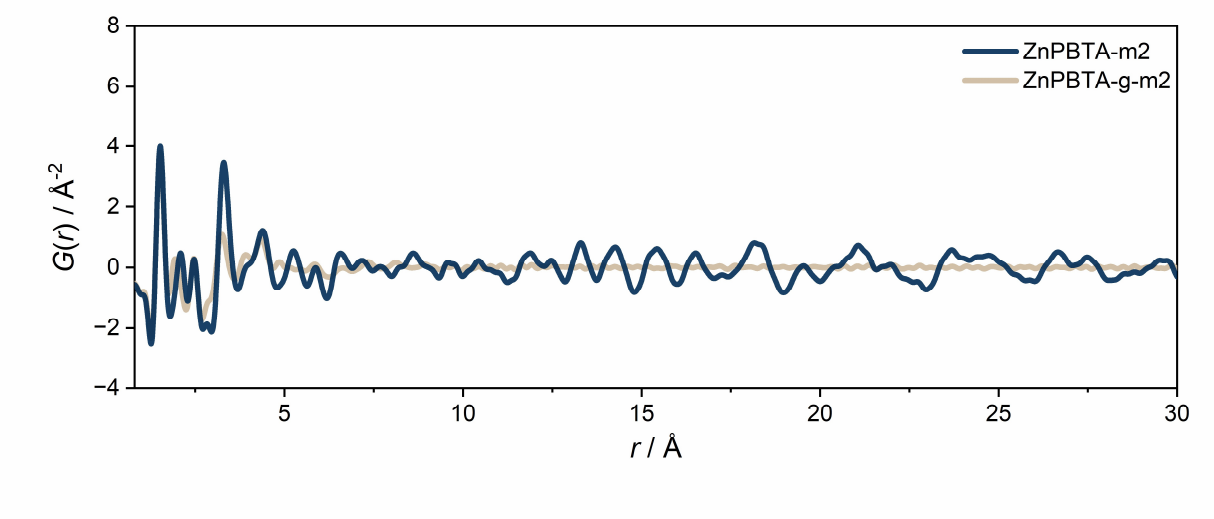

Figure S22. Pair distribution function (PDF) of ZnPBTA-m2 and ZnPBTA-g-m2 with extended range.

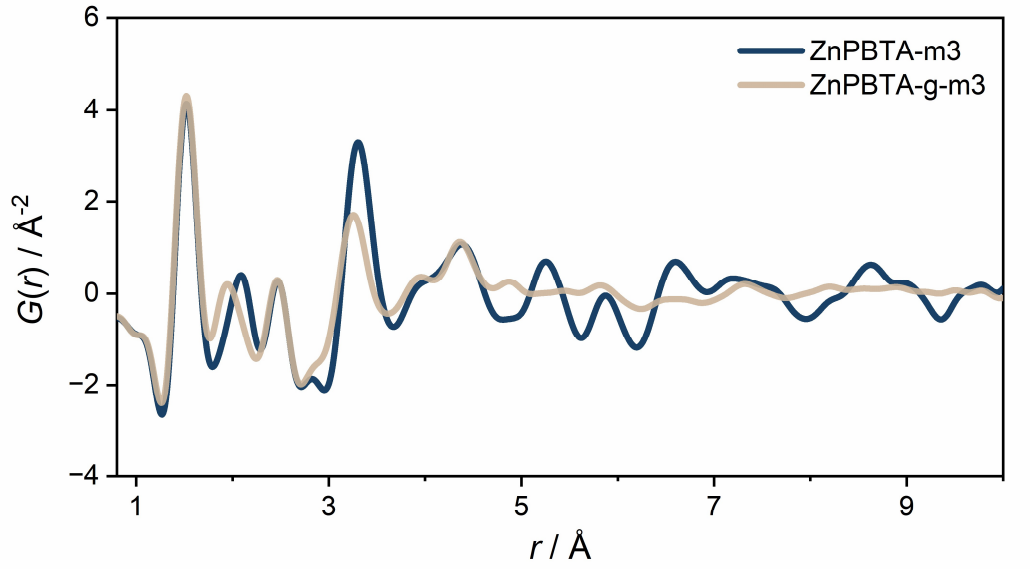

Figure S23. Pair distribution function (PDF) of ZnPBTA-m3 and ZnPBTA-g-m3.

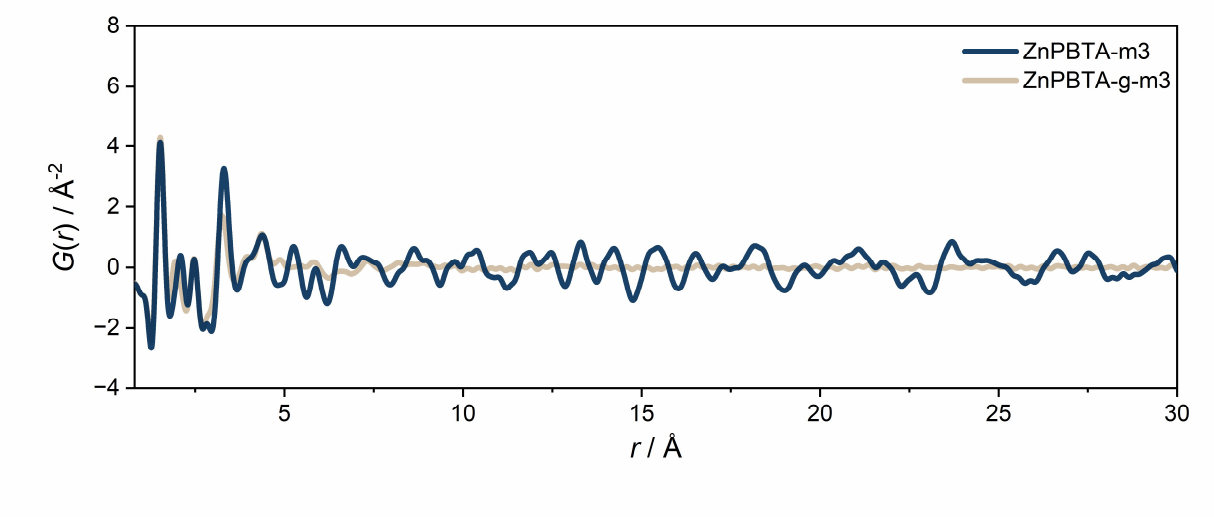

Figure S24. Pair distribution function (PDF) of ZnPBTA-m3 and ZnPBTA-g-m3 with extended range.

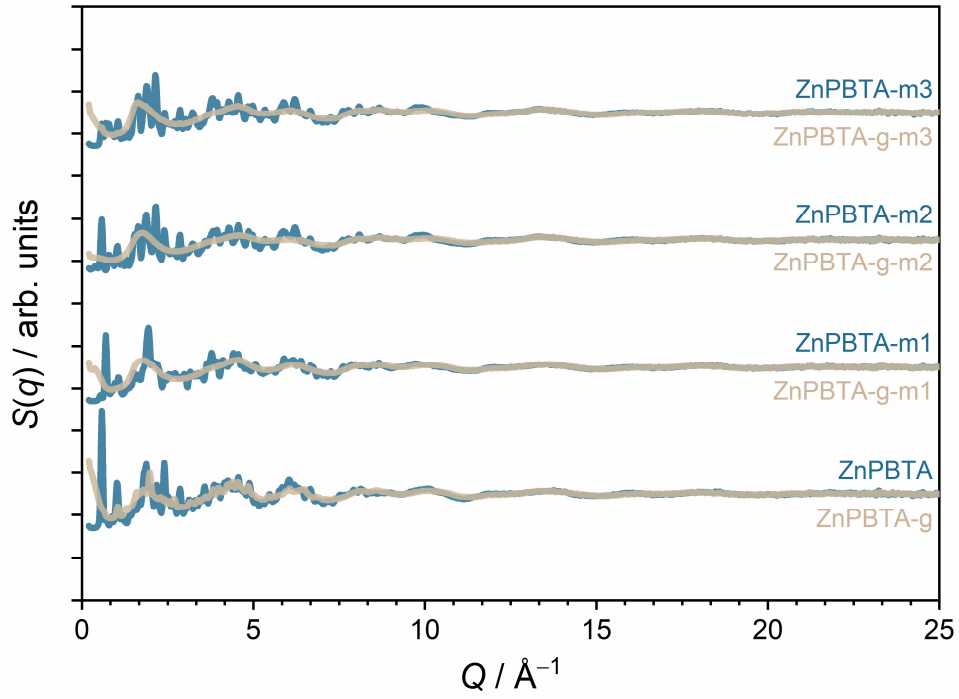

Figure S25. The structure factor, *S*(q), profiles of ZnPBTA, ZnPBTA-g, ZnPBTA-m1, ZnPBTA-g-m1, ZnPBTA-m2, ZnPBTA-g-m2, ZnPBTA-m3, and ZnPBTA-g-m3. Note that ZnPBTA-g exhibits a small degree of recrystallization due to its fast crystallization under ambient conditions.[11]

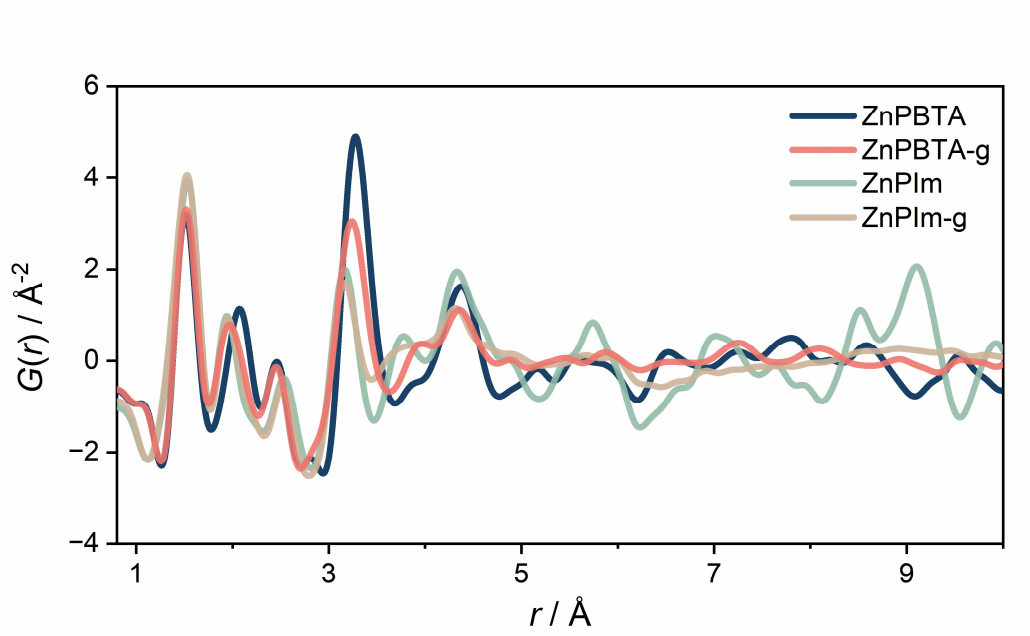

Figure S26. Pair distribution function (PDF) of ZnPBTA, ZnPBTA-g, ZnPIm, and ZnPIm-g. Data for ZnPIm and ZnPIm-g are obtained from ref. [12].

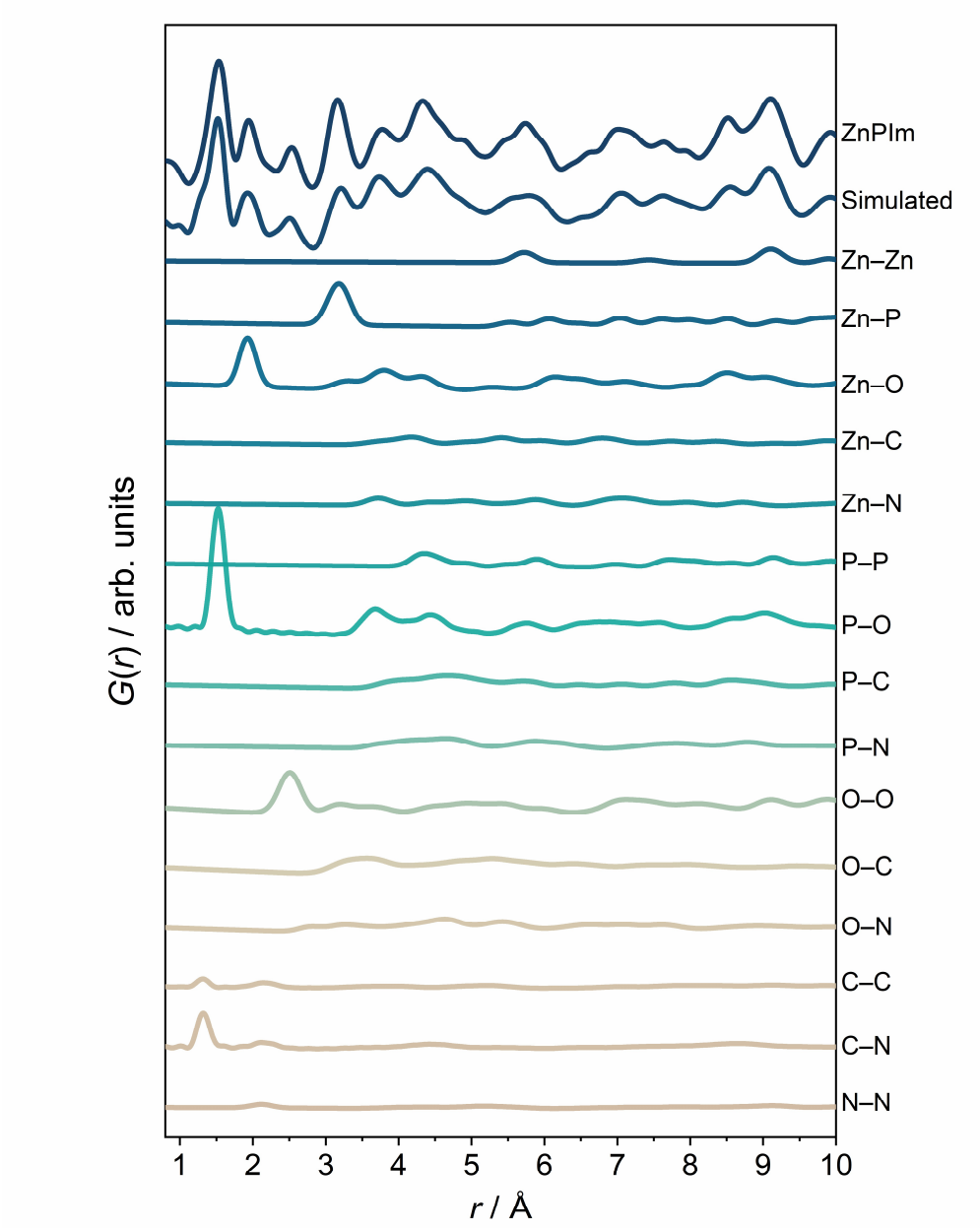

Figure S27. Pair distribution function (PDF), simulated PDF, and partial PDF of ZnPIm. PDF data for ZnPIm and ZnPIm-g are obtained from ref. [12]. Single crystal structure of ZnPIm for simulated PDF results are obtained from ref. [13].

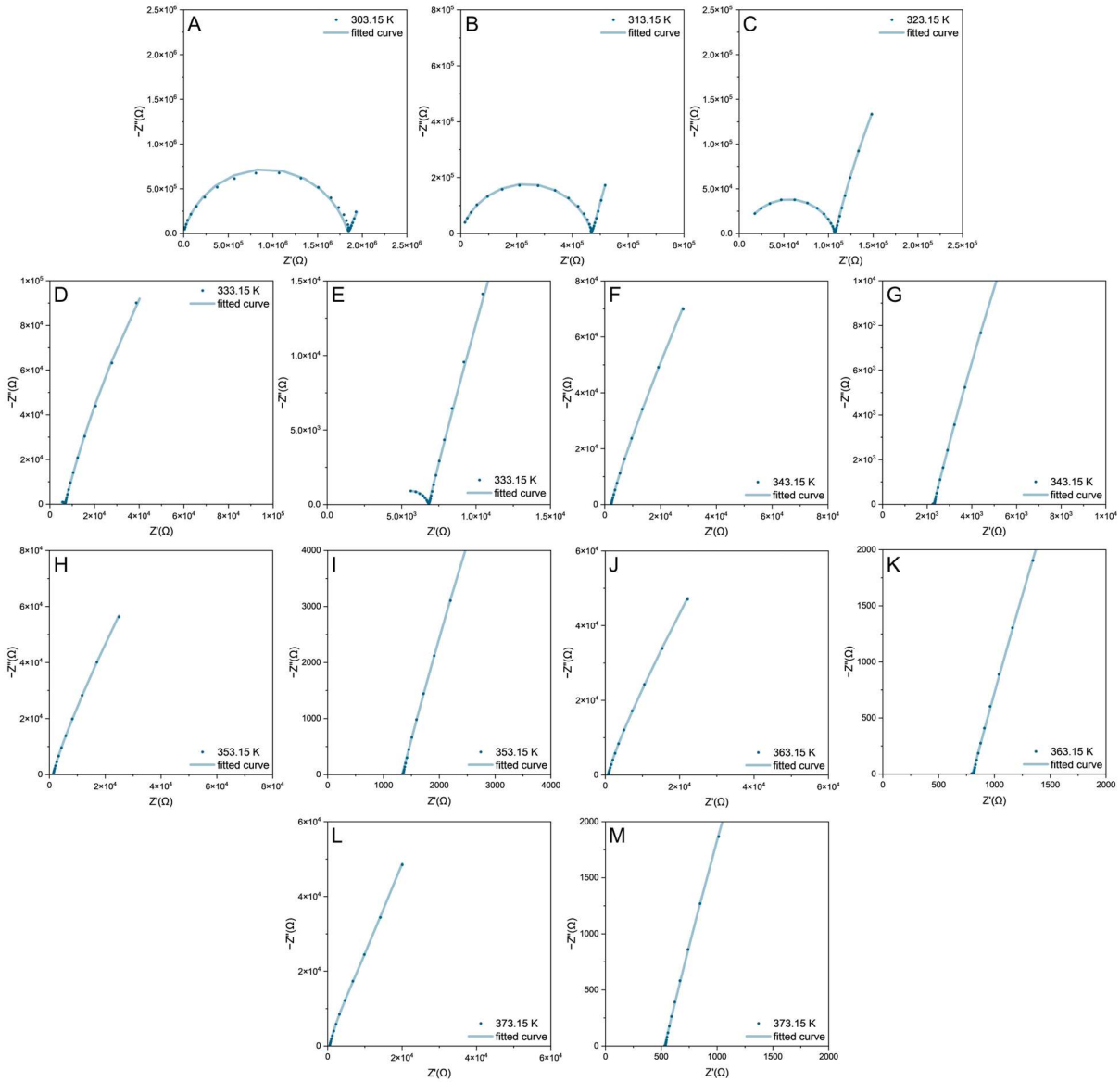

Figure S28. Nyquist plots of ZnPBTA at various temperatures under anhydrous conditions. The sample has a diameter of 5 mm and a thickness of 1.21 mm. The data were fitted using the R_1+(R_2Q_1) equivalent circuit model, where R_1 represents the bulk resistance, while R_2 and Q_1 correspond to interfacial resistances and constant phase elements, respectively. For data between 303.15 and 333.15 K, the (R_1Q_1)+(R_2Q_2) equivalent circuit model was used, with R_1 representing bulk resistance.[5] Fitting parameters are available in Table S10.

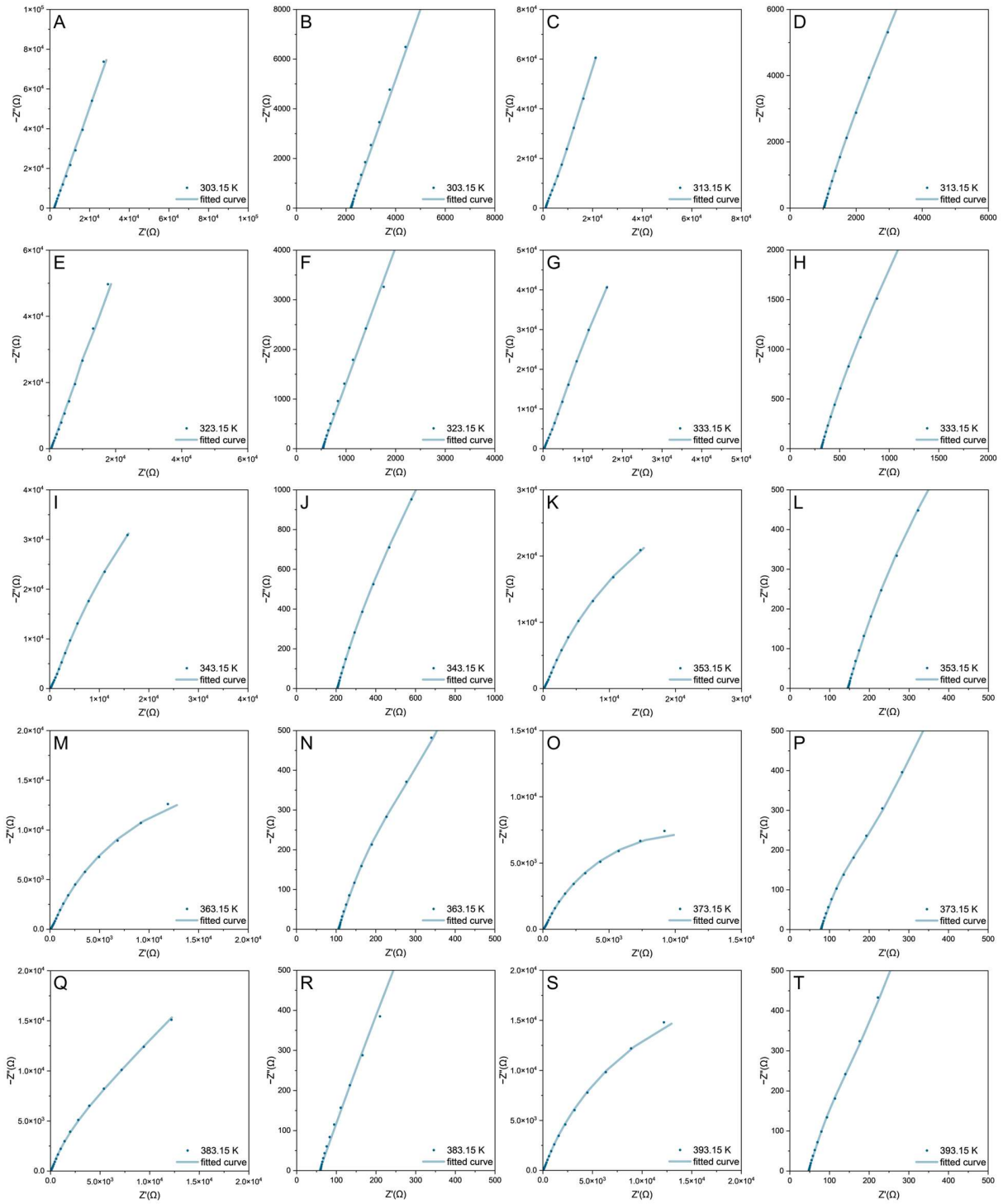

Figure S29. Nyquist plots of ZnPBTA-g at various temperatures under anhydrous conditions. The sample has a diameter of 7 mm and a thickness of 1.45 mm. The data were fitted using the R_1+(R_2Q_1) equivalent circuit model, where R_1 represents the bulk resistance, while R_2 and Q_1 correspond to interfacial resistances and constant phase elements, respectively.[5] Fitting parameters are available in Table S11.

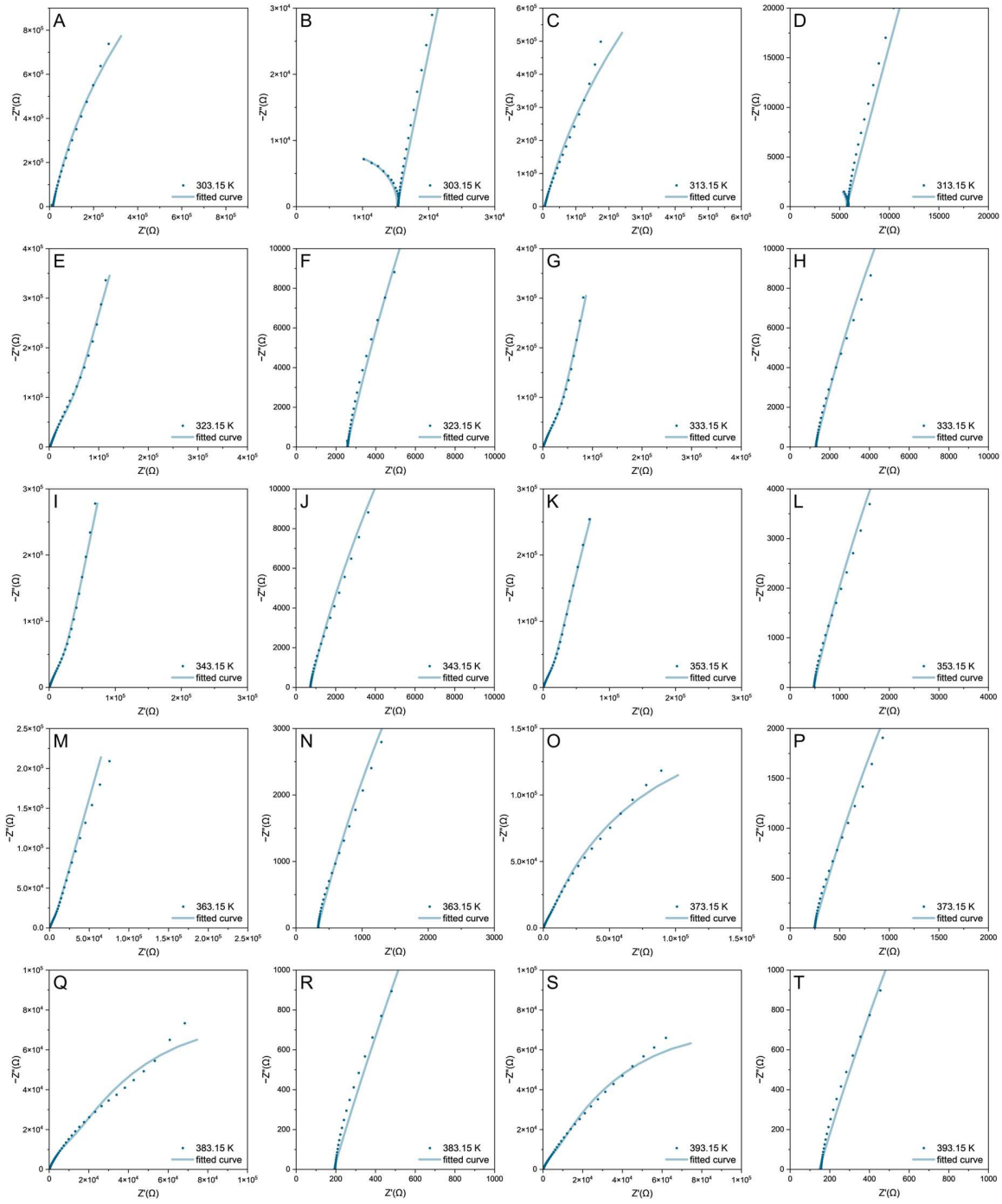

Figure S30. Nyquist plots of ZnPBTA-g-m1 at various temperatures under anhydrous conditions. The sample has a diameter of 5 mm and a thickness of 4.0 mm. The data were fitted using the R_1+(R_2Q_1)+(R_3Q_2) equivalent circuit model, where R_1 represents the bulk resistance, while R_2, R_3, Q_1, and Q_2 correspond to interfacial resistances and constant phase elements, respectively. For data at 303.15 and 313.15 K, the (R_1Q_1)+(R_2Q_2) equivalent circuit model was used, with R_1 representing bulk resistance. Fitting parameters are available in Table S12.

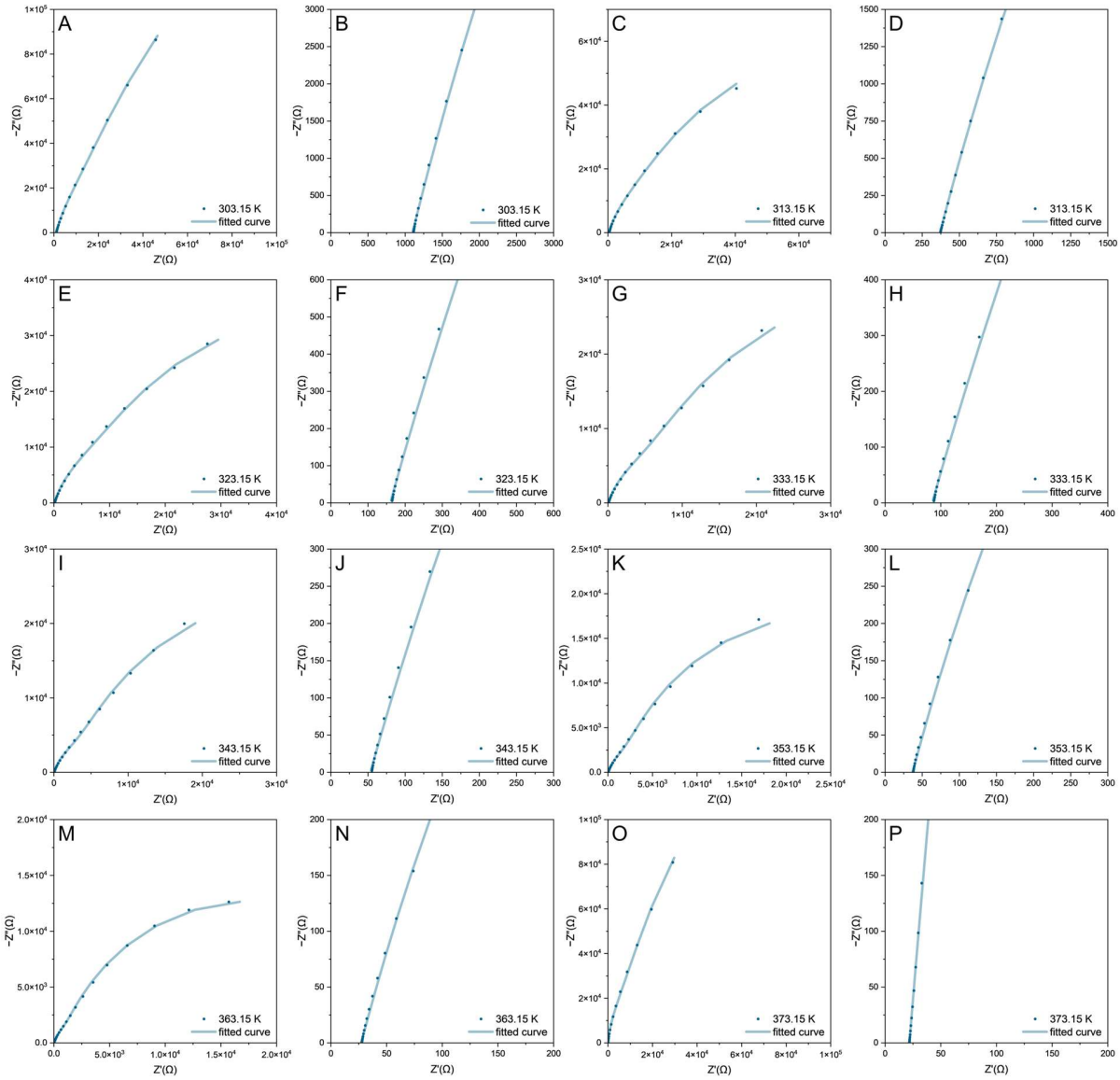

Figure S31. Nyquist plots of ZnPBTA-g-m2 at various temperatures under anhydrous conditions. The sample has a diameter of 7 mm and a thickness of 1.46 mm. The data were fitted using the R_1+(R_2Q_1)+(R_3Q_2) equivalent circuit model, where R_1 represents the bulk resistance, while R_2, R_3, Q_1, and Q_2 correspond to interfacial resistances and constant phase elements, respectively. Fitting parameters are available in Table S13.

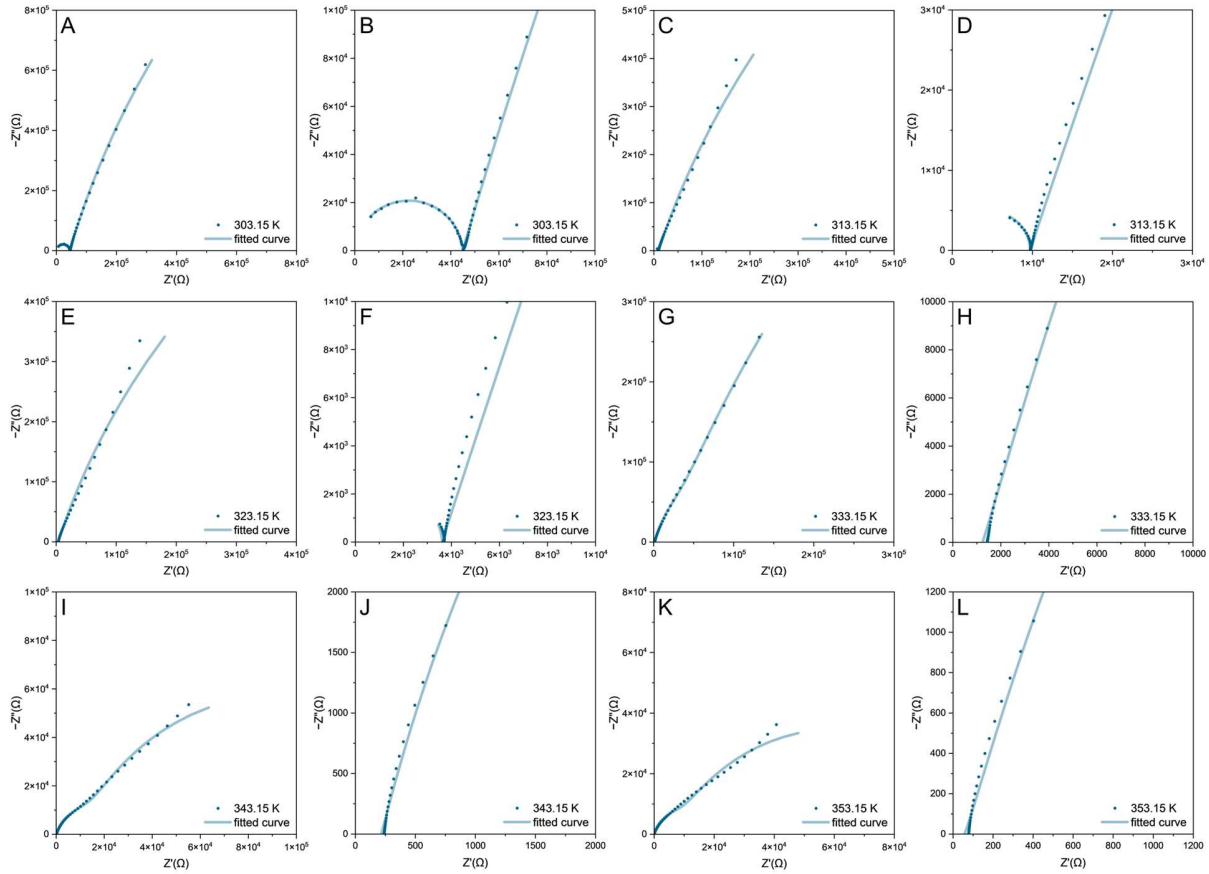

Figure S32. Nyquist plots of ZnPBTA-g-m3 at various temperatures under anhydrous conditions. The sample has a diameter of 5 mm and a thickness of 4.0 mm. The data were fitted using the R_1+(R_2Q_1)+(R_3Q_2) equivalent circuit model, where R_1 represents the bulk resistance, while R_2, R_3, Q_1, and Q_2 correspond to interfacial resistances and constant phase elements, respectively. For data at 303.15, 313.15, and 323.15 K, the (R_1Q_1)+(R_2Q_2) equivalent circuit model was used, with R_1 representing bulk resistance. Fitting parameters are available in Table S14.

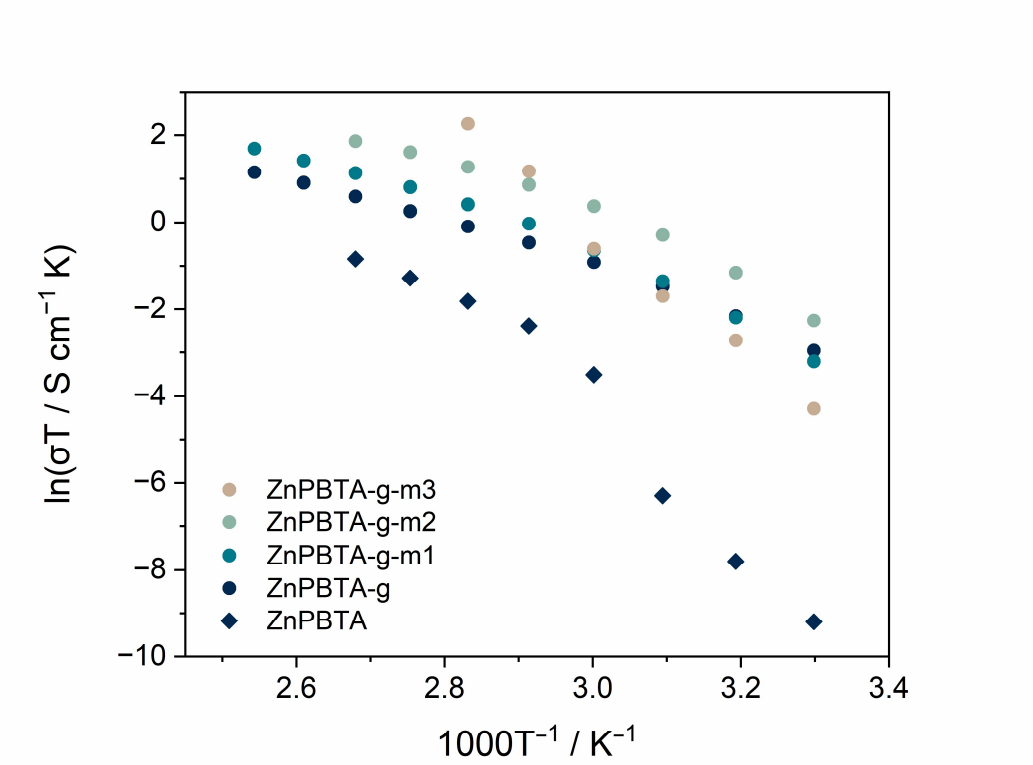

Figure S33. Arrhenius plots of the proton conductivity for ZnPBTA, ZnPBTA-g, ZnPBTA-g-m1, ZnPBTA-g-m2, and ZnPBTA-g-m3 under anhydrous conditions.

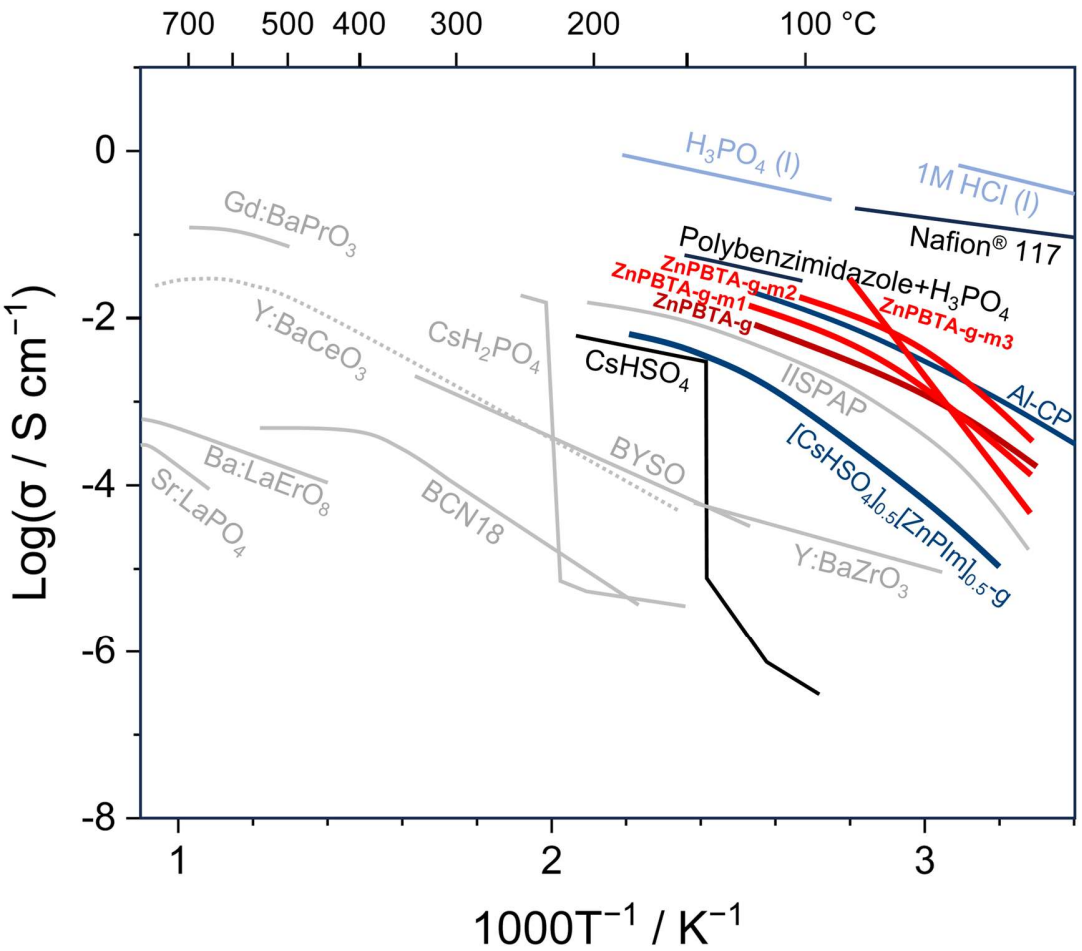

Figure S34. Proton conductivity of ZnPBTA, ZnPBTA-g, ZnPBTA-g-m1, ZnPBTA-g-m2, and ZnPBTA-g-m3 (plotted as red lines) under anhydrous conditions, compared with selected proton conductors from ref. [14]. The plot also includes anhydrous proton conductivity of a coordination polymer glass synthesized from a protic ionic liquid, $(dema)_{0.9}[Al(H_2O)_{1.8}\text{-}(H_2PO_4)_{3.9}(H_3PO_4)_{1.1}]$ (Al-CP),[15] and a binary $CsHSO_4$-coordination polymer glass, $[CsHSO_4]_{0.5}[ZnPIm]_{0.5}$-g.[16]

Supplementary tables

Table S1. Synthesis of CPs in this work.

	ZnO	1,2,3-benzotriazole	H_3PO_4 (85% in H_2O)	At 393 K	After cooling to 298 K
ZnPBTA	15.75 mmol (1281.7 mg)	5.25 mmol (625.4 mg)	31.5 mmol (2163 μL)	white liquid	white solid
ZnPBTA-m1	15.75 mmol (1281.7 mg)	5.25 mmol (625.4 mg)	40.7 mmol (2794 μL)	transparent liquid	transparent viscous liquid
ZnPBTA-m2	15.75 mmol (1281.7 mg)	5.25 mmol (625.4 mg)	49.9 mmol (3425 μL)	transparent liquid	transparent viscous liquid
ZnPBTA-m3	15.75 mmol (1281.7 mg)	5.25 mmol (625.4 mg)	59.1 mmol (4056 μL)	transparent liquid	transparent viscous liquid

Table S2. Zn and P mol fraction of dehydrated samples from Inductively Coupled Plasma-Optical Emission Spectroscopy (ICP-OES).

	Zn/P mol fraction	Standard deviation	Expected Zn/P mol fraction
ZnPBTA	0.470	0.006	0.500
ZnPBTA-m1	0.364	0.003	0.387
ZnPBTA-m2	0.294	0.004	0.316
ZnPBTA-m3	0.253	0.005	0.267

Table S3. Melting temperatures at peak position, endset temperature, and overall enthalpies associated with the flux melting of ZnPBTA, ZnPBTA-m1, ZnPBTA-m2, and ZnPBTA-m3, as determined from DSC thermograms recorded under a flowing N_2 atmosphere at a heating rate of 10 K min^{-1} (Figure S8). The molar enthalpies are calculated based on the estimated theoretical molar units: $Zn_3(H_2PO_4)_x](C_6H_5N_3)$.

	$T_{m,\ peak}$ / K	T_{endset} / K	ΔH / J g^{-1}	ΔH / kJ mol^{-1}
ZnPBTA	394.6	399.1	19.5	17.5
ZnPBTA-m1	384.7	390.5	19.0	20.3
ZnPBTA-m2	359.4	364.7	32.1	39.7
ZnPBTA-m3	370.7	374.1	29.8	41.9

Table S4. MYEGA $[\log_{10}\eta(T) = \log_{10}\eta_\infty + \frac{K}{T}\exp(\frac{C}{T})]$ fitting parameters.

	η_∞	K	C
ZnPBTA-g	308.2 ± 126	0.009 ± 0.017	3532.9 ± 126
ZnPBTA-g-m1	2.966 ± 0.339	0.017 ± 0.004	3358.4 ± 65.8
ZnPBTA-g-m2	0.195 ± 0.036	0.653 ± 0.144	2226.5 ± 59.5
ZnPBTA-g-m3	0.222 ± 0.072	0.172 ± 0.102	2463.2 ± 157

Table S5. Predicted and measured Zn···Zn pair distances of ZnPBTA, ZnPBTA-m1, ZnPBTA-m2, and ZnPBTA-m3. The predicted values were calculated from the crystal structure of ZnPBTA, collected at 100 K.[5]

	Zn···Zn^{1st}	**Zn···Zn^{2nd}**	**Zn···Zn^{3nd}**
Predicted	3.19 Å	5.37 Å	7.48 Å
ZnPBTA	3.3 Å	5.2 and 5.5 Å[a]	7.2 and 7.8 Å[ab]
ZnPBTA-m1	3.3 Å	5.3 Å	7.5 Å
ZnPBTA-m2	3.3 Å	5.3 Å	7.2 and 7.7 Å[b]
ZnPBTA-m3	3.3 Å	5.3 Å	7.2 and 7.6Å[b]

[a]Peak splitting in ZnPBTA is attributed to deformation of the Zn^{2+} octahedral coordination sphere upon dehydration.
[b]Peaks contains contributions from Zn···P, Zn···O, P···O, and O···O.

Table S6. Predicted and measured Zn···Zn pair distances of ZnPBTA-g, ZnPBTA-g-m1, ZnPBTA-g-m2, and ZnPBTA-g-m3. The predicted values were calculated from the crystal structure of ZnPIm, collected at 243 K.[13]

	Zn···Zn^{1st}
Predicted	5.73 Å
ZnPBTA-g	5.9 Å
ZnPBTA-g-m1	5.8 Å
ZnPBTA-g-m2	5.8 Å
ZnPBTA-g-m3	5.8 Å

Table S7. Anhydrous proton conductivity at 373 K of representative coordination polymers and metal-organic frameworks.

Compound	Estimated proton conductivity σ / mS cm^{-1}	Ref.
ZnPBTA	1.2	This work
ZnPBTA-g	4.8	This work
ZnPBTA-g-m1	8.3	This work
ZnPBTA-g-m2	17.2	This work
Coordination polymer glasses		
$[Mn(H_2PO_4)_2(1,2,4\text{-triazole})_2]$-g (240 min ball milling)	3.9×10^{-4}	[17]
$[Cd(H_2PO_4)_2(1,2,4\text{-triazole})_2]$-g (240 min ball milling)	1.3×10^{-2}	[18]
$Zn(HPO_4)(H_2PO_4)_2](H_2Im)_2$-g (ZnPIm-g)	6.9×10^{-2}	[16]
$[CsHSO_4]_{0.5}[ZnPIm]_{0.5}$-g	0.6	[16]
$(dema)_{0.45}[Zn_{0.75}(H_{2.35}PO_4)_3]$	12.1	[19]
$(dema)_{0.9}[Al(H_2O)_{1.8}(H_2PO_4)_{3.9}(H_3PO_4)_{1.1}]$	13.6	[15]
Coordination polymers / Metal-organic frameworks		
$[Mn(H_2PO_4)_2(1,2,4\text{-triazole})_2]$	3.9×10^{-6}	[17]
$[Cd(H_2PO_4)_2(1,2,4\text{-triazole})_2]$	1.4×10^{-5}	[18]
$[Co(HPO_3)_2][H_2DABCO]$	1.2×10^{-4}	[20]
$[Zn(H_2PO_4)_2(1,2,4\text{-triazole})_2]$	1.8×10^{-2}	[21]
$[(Me_2NH_2)_3(SO_4)]_2[Zn_2(ox)_3]$	9.9×10^{-2}	[22]
$Zn(HPO_4)(H_2PO_4)_2](H_2Im)_2$	0.14	[13]
$[Eu_2(CO_3)(ox)_2(H_2O)_2]\cdot 4H_2O$	0.82	[23]
$(Me_2NH_2)[Eu(L)]$ (H_4L=5-(phosphonomethyl)isophthalic acid)	0.88	[24]
Guest-Encapsulated Metal-Organic Frameworks		
Imidazole @ [Al(μ_2-OH)(1,4-naphthalenedicarboxylate)]	9.6×10^{-3}	[25]
$(Tz)_{0.45}$ @ β-PCMOF2	0.16	[26]
Histamine @ [Al(μ_2-OH)(1,4-naphthalenedicarboxylate)]	0.72	[27]
H_3PO_4 @ $[Zn(H_2PO_4)_2(1,2,4\text{-triazole})_2]$	1.06	[28]
LiBr @ $(H_3O)[(UO_2)_4(2\text{-(phosphonomethyl)benzoate})_3(H_2O)_3]\cdot 0.5H_2O$	143.5	[29]

Table S8. VFT fitting parameters for proton conductivities.
VFT equation: $\sigma = \sigma_0 \exp[-(B/(T-T_0))]$. The fitting parameters include the pre-exponent factor (σ_0), the activation factor (B), and the ideal transition temperature (T_0).

	σ_0 / S cm^{-1}	B / K	T_0 / K	R^2
ZnPBTA-g	0.62 (± 0.24)	849 (± 134)	198 (± 13)	0.9996
ZnPBTA-g-m1	0.40 (± 0.09)	526 (± 57)	238 (± 7)	0.9998
ZnPBTA-g-m2	0.20 (± 0.03)	276 (± 22)	261 (± 4)	0.9999

Table S9. Volume and density measurements. The volume of containers A and B are 226.5 and 225.4 mm^3, respectively.

	measured volume (sample+container)	**sample volume**	**weight**	**density**
ZnPBTA-g (container A)	256.7 ± 0.2 mm^3	30.2 mm^3	61.7 mg	2.04 g/cm^3
ZnPBTA-g-m1 (container B)	270.1 ± 0.2 mm^3	44.7 mm^3	93.5 mg	2.09 g/cm^3
ZnPBTA-g-m2 (container A)	273.2 ± 0.2 mm^3	46.7 mm^3	99.9 mg	2.14 g/cm^3
ZnPBTA-g-m3 (container B)	243.7 ± 0.1 mm^3	18.3 mm^3	34.7 mg	1.90 g/cm^3

Table S10. Fitting parameters for ZnPBTA as shown in Figure S28 at different temperatures.

Temperature / K	R_1 / Ω	R_2 / Ω	Q_1 / $Fs^{\alpha-1}$	Q_2 / $Fs^{\alpha-1}$	χ^2 / |Z|
303.15	1.84×10^{6} ± 0.537	1.23×10^{18} ± 1.04×10^{23}	3.96×10^{-12} ± 3.8×10^{-14}	9.70×10^{-5} ± 1.8×10^{-11}	0.018
313.15	4.71×10^{5} ± 0.495	2.02×10^{7} ± 1.14×10^{5}	6.45×10^{-11} ± 2.5×10^{-15}	1.20×10^{-6} ± 1.4×10^{-10}	0.002
323.15	1.08×10^{5} ± 0.384	8.79×10^{18} ± 1.42×10^{24}	1.91×10^{-10} ± 3.2×10^{-14}	1.57×10^{-6} ± 3.7×10^{-11}	0.009
333.15	6816 ± 0.439	9.54×10^{5} ± 627	1.30×10^{-9} ± 1.6×10^{-13}	2.13×10^{-6} ± 4.6×10^{-10}	0.006
343.15	2288 ± 0.238	7.30×10^{5} ± 487	-	2.76×10^{-6} ± 6.5×10^{-10}	0.007
353.15	1334 ± 0.239	4.41×10^{5} ± 204	-	3.34×10^{-6} ± 9.4×10^{-10}	0.015
363.15	805 ± 0.240	3.72×10^{5} ± 168	-	3.96×10^{-6} ± 1.3×10^{-9}	0.028
373.15	528.3 ± 0.240	5.00×10^{5} ± 373	-	3.94×10^{-6} ± 1.3×10^{-9}	0.044

Table S11. Fitting parameters for ZnPBTA-g as shown in Figure S29 at different temperatures.

Temperature / K	R_1 / Ω	R_2 / Ω	Q_1 / $Fs^{\alpha-1}$	χ^2 / |Z|
303.15	2198 ± 0.280	6.20×10^{6} ± 2.57×10^{4}	1.81×10^{-5} ± 1.7×10^{-9}	0.008
313.15	1020 ± 0.292	2.91×10^{7} ± 8.60×10^{5}	2.23×10^{-5} ± 2.5×10^{-9}	0.011
323.15	526.8 ± 0.306	2.76×10^{7} ± 1.09×10^{6}	2.71×10^{-5} ± 3.8×10^{-9}	0.017
333.15	302.8 ± 0.325	4.05×10^{6} ± 258×10^{4}	3.29×10^{-5} ± 5.9×10^{-9}	0.019
343.15	195.4 ± 0.346	4.21×10^{5} ± 367	4.02×10^{-5} ± 9.5×10^{-9}	0.023
353.15	139.1 ± 0.305	1.18×105 ± 104	4.95×10^{-5} ± 1.6×10^{-8}	0.042
363.15	101.9 ± 0.357	4.66×10^{4} ± 40.2	6.24×10^{-5} ± 2.8×10^{-8}	0.061
373.15	76.8 ± 0.362	2.34×10^{4} ± 20.3	7.69×10^{-5} ± 4.5×10^{-8}	0.073
383.15	58.2 ± 0.201	4.07×10^{4} ± 23.2	5.60×10^{-5} ± 2.1×10^{-8}	0.138
393.15	47.1 ± 0.200	5.14×10^{4} ± 32.3	5.91×10^{-5} ± 2.2×10^{-8}	0.090

Table S12. Fitting parameters for ZnPBTA-m1-g as shown in Figure S30 at different temperatures.

Temperature / K	R_1 / Ω	R_2 / Ω	R_3 / Ω	Q_1 / $Fs^{\alpha-1}$	Q_2 / $Fs^{\alpha-1}$	χ^2 / |Z|
303.15	15260 ± 9.93	4.41×10^{6} ± 124	-	8.25×10^{-12} ± 1.2×10^{-14}	1.71×10^{-6} ± 1.0×10^{-11}	0.036
313.15	5637 ± 0.176	3.45×10^{6} ± 125	-	1.12×10^{-11} ± 9.2×10^{-14}	2.44×10^{-6} ± 2.3×10^{-11}	0.181
323.15	2543 ± 0.212	1.03×10^{7} ± 6.44×10^{4}	4.55×10^{4} ± 99.3	4.32×10^{-6} ± 1.0×10^{-9}	6.16×10^{-6} ± 9.3×10^{-9}	0.032
333.15	1283 ± 0.210	5.63×10^{30} ± 228×10^{36}	2.54×10^{4} ± 17.2	4.88×10^{-6} ± 2.7×10^{-10}	7.36×10^{-6} ± 4.4×10^{-9}	0.035
343.15	712.2 ± 0.211	4.27×10^{42} ± 1.82×10^{48}	1.72×10^{4} ± 13.2	5.32×10^{-6} ± 3.3×10^{-10}	8.25×10^{-6} ± 5.7×10^{-9}	0.033
353.15	476.1 ± 0.165	8.52×10^{4} ± 39.0	9.90×10^{3} ± 21.6	1.86×10^{-5} ± 9.6×10^{-9}	5.36×10^{-6} ± 8.4×10^{-9}	0.302
363.15	329.5 ± 0.167	2.82×10^{9} ± 3.93×10^{7}	3.68×10^{3} ± 10.2	6.62×10^{-6} ± 2.4×10^{-9}	1.11×10^{-6} ± 3.5×10^{-8}	0.067
373.15	244.9 ± 0.169	3.52×10^{5} ± 109	4.14×10^{3} ± 13.5	7.68×10^{-6} ± 3.1×10^{-10}	1.05×10^{-5} ± 3.5×10^{-8}	0.102
383.15	190.0 ± 0.169	1.84×10^{5} ± 150	1.23×10^{4} ± 42.0	1.22×10^{-5} ± 1.1×10^{-8}	9.69×10^{-6} ± 1.9×10^{-8}	0.177
393.15	147.7 ± 0.171	1.81×10^{5} ± 70.4	5.65×10^{3} ± 20.5	1.10×10^{-5} ± 2.6×10^{-9}	9.62×10^{-6} ± 2.6×10^{-8}	0.209

Table S13. Fitting parameters for ZnPBTA-m2-g as shown in Figure S31 at different temperatures.

Temperature / K	R_1 / Ω	R_2 / Ω	R_3 / Ω	Q_1 / $Fs^{\alpha-1}$	Q_2 / $Fs^{\alpha-1}$	χ^2 / |Z|
303.15	1105 ± 0.391	4.96×10^{5} ± 3.41×10^{3}	9.64×10^{3} ± 229	1.50×10^{-5} ± 4.3×10^{-8}	3.63×10^{-5} ± 5.9×10^{-7}	0.003
313.15	370.8 ± 0.376	1.46×10^{5} ± 168	8.97×10^{3} ± 242	2.26×10^{-5} ± 1.2×10^{-7}	3.44×10^{-6} ± 6.5×10^{-7}	0.007
323.15	160.2 ± 0.366	8.92×10^{4} ± 324	6.29×10^{3} ± 126	3.20×10^{-5} ± 9.4×10^{-10}	3.51×10^{-5} ± 4.9×10^{-7}	0.014
333.15	86.7 ± 0.338	9.28×10^{4} ± 291	2.08×10^{3} ± 11.4	3.83×10^{-6} ± 6.1×10^{-10}	3.20×10^{-5} ± 6.1×10^{-8}	0.083
343.15	54.4 ± 0.343	6.03×10^{4} ± 216	3.21×10^{3} ± 44.2	4.61×10^{-6} ± 1.5×10^{-7}	3.30×10^{-5} ± 3.4×10^{-7}	0.038
353.15	37.3 ± 0.325	4.65×10^{4} ± 105	1.59×10^{3} ± 27.8	4.57×10^{-5} ± 7.4×10^{-8}	3.69×10^{-5} ± 5.5×10^{-7}	0.036
363.15	27.3 ± 0.317	3.38×10^{4} ± 28.0	729 ± 17.1	4.62×10^{-5} ± 4.3×10^{-8}	4.74×10^{-5} ± 1.4×10^{-6}	0.023
373.15	21.9 ± 0.212	4.22×10^{5} ± 2.69×10^{3}	9.54×10^{3} ± 115	1.82×10^{-7} ± 4.3×10^{-8}	4.61×10^{-5} ± 4.7×10^{-7}	0.003

Table S14. Fitting parameters for ZnPBTA-m3-g as shown in Figure S32 at different temperatures.

Temperature / K	R_1 / Ω	R_2 / Ω	R_3 / Ω	Q_1 / $Fs^{\alpha-1}$	Q_2 / $Fs^{\alpha-1}$	χ^2 / |Z|
303.15	45124 ± 0.192	5.31×10^{6} ± 194	-	2.13×10^{-11} ± 6.1×10^{-15}	2.02×10^{-6} ± 1.6×10^{-11}	0.011
313.15	9657 ± 0.182	3.40×10^{6} ± 91.8	-	1.02×10^{-11} ± 2.9×10^{-14}	3.04×10^{-6} ± 3.8×10^{-11}	0.065
323.15	3615 ± 0.156	2.29×10^{6} ± 31.5	-	9.18×10^{-12} ± 5.3×10^{-15}	3.53×10^{-6} ± 5.2×10^{-11}	0.160
333.15	1427 ± 0.159	1.44×10^{6} ± 1126	3.63×10^{5} ± 74.8	5.07×10^{-6} ± 8.2×10^{-10}	6.44×10^{-6} ± 9.9×10^{-9}	0.036
343.15	229.2 ± 0.165	1.66×10^{5} ± 128	1.11×10^{4} ± 19.7	1.46×10^{-5} ± 6.7×10^{-9}	4.69×10^{-6} ± 5.1×10^{-9}	0.174
353.15	75.88 ± 0.168	8.52×10^{4} ± 39.0	9.90×10^{3} ± 21.6	1.86×10^{-5} ± 9.6×10^{-9}	5.36×10^{-6} ± 8.4×10^{-9}	0.302

References

[1] S. Kohara, M. Itou, K. Suzuya, Y. Inamura, Y. Sakurai, Y. Ohishi, M. Takata, "Structural studies of disordered materials using high-energy x-ray diffraction from ambient to extreme conditions" *J. Phys. Condens. Matter.* **2007**, *19*, 506101.

[2] T. E. Faber, J. M. Ziman, "A theory of the electrical properties of liquid metals" *Philos. Mag.* **1965**, *11*, 153–173.

[3] E. Lorch, "Neutron diffraction by germania, silica and radiation-damaged silica glasses" *J. Phys. C: Solid State Phys.* **1969**, *2*, 229–237.

[4] C. L. Farrow, P. Juhas, J. W. Liu, D. Bryndin, E. S. Božin, J. Bloch, T. Proffen, S. J. L. Billinge, "PDFfit2 and PDFgui: computer programs for studying nanostructure in crystals" *J. Phys.: Condens. Matter* **2007**, *19*, 335219.

[5] N. Ma, S. Kosasang, A. Yoshida, S. Horike, "Proton-conductive coordination polymer glass for solid-state anhydrous proton batteries" *Chem. Sci.* **2021**, *12*, 5818–5824.

[6] R. H. Blessing, "New analysis of the neutron diffraction data for anhydrous orthophosphoric acid and the structure of H_3PO_4 molecules in crystals" *Acta Cryst.* **1988**, *44*, 334–340.

[7] Y. H. Lei, N. Sheng, A. Hyono, M. Ueda, T. Ohtsuka, "Effect of benzotriazole (BTA) addition on Polypyrrole film formation on copper and its corrosion protection" *Prog. Org. Coat.* **2014**, *77*, 339–346.

[8] S. Pili, P. Rought, D. I. Kolokolov, L. Lin, I. da Silva, Y. Cheng, C. Marsh, I. P. Silverwood, V. García Sakai, M. Li, J. J. Titman, L. Knight, L. L. Daemen, A. J. Ramirez-Cuesta, C. C. Tang, A. G. Stepanov, S. Yang, M. Schröder, "Enhancement of Proton Conductivity in Nonporous Metal–Organic Frameworks: The Role of Framework Proton Density and Humidity" *Chem. Mater.* **2018**, *30*, 7593–7602.

[9] K. I. Hadjiivanov, D. A. Panayotov, M. Y. Mihaylov, E. Z. Ivanova, K. K. Chakarova, S. M. Andonova, N. L. Drenchev, "Power of Infrared and Raman Spectroscopies to Characterize Metal-Organic Frameworks and Investigate Their Interaction with Guest Molecules" *Chem. Rev.* **2020**, *121*, 1286–1424.

[10] J. N. Yankwa Djobo, R. Y. Nkwaju, "Preparation of acid aluminum phosphate solutions for metakaolin phosphate geopolymer binder" *RSC Adv.* **2021**, *11*, 32258–32268.

[11] D. Umeyama, S. Horike, M. Inukai, T. Itakura, S. Kitagawa, "Reversible Solid-to-Liquid Phase Transition of Coordination Polymer Crystals" *J. Am. Chem. Soc.* **2015**, *137*, 864–870.

[12] N. Ma, S. Impeng, S. Bureekaew, N. Morozumi, M.-a. Haga, S. Horike, "Photoexcited Anhydrous Proton Conductivity in Coordination Polymer Glass" *J. Am. Chem. Soc.* **2023**, *145*, 9808–9814.

[13] S. Horike, D. Umeyama, M. Inukai, T. Itakura, S. Kitagawa, "Coordination-Network-Based Ionic Plastic Crystal for Anhydrous Proton Conductivity" *J. Am. Chem. Soc.* **2012**, *134*, 7612–7615.

[14] T. Norby, "Solid-state protonic conductors: principles, properties, progress and prospects" *Solid State Ion.* **1999**, *125*, 1–11.

[15] K. Takahashi, T. Ogawa, T. Itakura, K. Kami, S. Horike, "Water-Stable Al(III) Coordination Polymer Glass with High Proton Conductivity toward Stable Electrolytes in a Fuel Cell" *ACS Appl. Energy Mater.* **2024**, *7*, 11937–11945.
[16] N. Ma, N. Horike, L. Lombardo, S. Kosasang, K. Kageyama, C. Thanaphatkosol, K. Kongpatpanich, K.-i. Otake, S. Horike, "Eutectic $CsHSO_4$-Coordination Polymer Glasses with Superprotonic Conductivity" *J. Am. Chem. Soc.* **2022**, *144*, 18619–18628.
[17] Y. Ohara, A. Hinokimoto, W. Chen, T. Kitao, Y. Nishiyama, Y.-I. Hong, S. Kitagawa, S. Horike, "Formation of coordination polymer glass by mechanical milling: dependence on metal ions and molecular doping for H^+ conductivity" *Chem. Commun.* **2018**, *54*, 6859–6862.
[18] W. Chen, S. Horike, D. Umeyama, N. Ogiwara, T. Itakura, C. Tassel, Y. Goto, H. Kageyama, S. Kitagawa, "Glass Formation of a Coordination Polymer Crystal for Enhanced Proton Conductivity and Material Flexibility" *Angew. Chem. Int. Ed.* **2016**, *55*, 5195–5200.
[19] T. Ogawa, K. Takahashi, T. Kurihara, S. S. Nagarkar, K. Ohara, Y. Nishiyama, S. Horike, "Network Size Control in Coordination Polymer Glasses and Its Impact on Viscosity and H^+ Conductivity" *Chem. Mater.* **2022**, *34*, 5832–5841.
[20] S.-S. Yu, S.-X. Liu, H.-B. Duan, "Dielectric response and anhydrous proton conductivity in a chiral framework containing a non-polar molecular rotor" *Dalton Trans.* **2015**, *44*, 20822–20825.
[21] D. Umeyama, S. Horike, M. Inukai, T. Itakura, S. Kitagawa, "Inherent Proton Conduction in a 2D Coordination Framework" *J. Am. Chem. Soc.* **2012**, *134*, 12780–12785.
[22] S. S. Nagarkar, S. M. Unni, A. Sharma, S. Kurungot, S. K. Ghosh, "Two-in-One: Inherent Anhydrous and Water-Assisted High Proton Conduction in a 3D Metal–Organic Framework" *Angew. Chem. Int. Ed.* **2014**, *53*, 2638–2642.
[23] Q. Tang, Y. Liu, S. Liu, D. He, J. Miao, X. Wang, G. Yang, Z. Shi, Z. Zheng, "High Proton Conduction at above 100 °C Mediated by Hydrogen Bonding in a Lanthanide Metal–Organic Framework" *J. Am. Chem. Soc.* **2014**, *136*, 12444–12449.
[24] Y.-S. Wei, X.-P. Hu, Z. Han, X.-Y. Dong, S.-Q. Zang, T. C. W. Mak, "Unique Proton Dynamics in an Efficient MOF-Based Proton Conductor" *J. Am. Chem. Soc.* **2017**, *139*, 3505–3512.
[25] S. Bureekaew, S. Horike, M. Higuchi, M. Mizuno, T. Kawamura, D. Tanaka, N. Yanai, S. Kitagawa, "One-dimensional imidazole aggregate in aluminium porous coordination polymers with high proton conductivity" *Nat. Mater.* **2009**, *8*, 831–836.
[26] J. A. Hurd, R. Vaidhyanathan, V. Thangadurai, C. I. Ratcliffe, I. L. Moudrakovski, G. K. H. Shimizu, "Anhydrous proton conduction at 150 °C in a crystalline metal–organic framework" *Nat. Chem.* **2009**, *1*, 705–710.
[27] D. Umeyama, S. Horike, M. Inukai, Y. Hijikata, S. Kitagawa, "Confinement of Mobile Histamine in Coordination Nanochannels for Fast Proton Transfer" *Angew. Chem. Int. Ed.* **2011**, *50*, 11706–11709.
[28] M. Inukai, S. Horike, T. Itakura, R. Shinozaki, N. Ogiwara, D. Umeyama, S. Nagarkar, Y. Nishiyama, M. Malon, A. Hayashi, T. Ohhara, R. Kiyanagi, S. Kitagawa, "Encapsulating Mobile Proton Carriers into Structural Defects in

Coordination Polymer Crystals: High Anhydrous Proton Conduction and Fuel Cell Application" *J. Am. Chem. Soc.* **2016**, *138*, 8505–8511.

[29] K. Zhang, G.-H. Wen, X.-J. Yang, D.-W. Lim, S.-S. Bao, M. Donoshita, L.-Q. Wu, H. Kitagawa, L.-M. Zheng, "Anhydrous Superprotonic Conductivity of a Uranyl-Based MOF from Ambient Temperature to 110 °C" *ACS Materials Lett.* **2021**, *3*, 744–751.